Economic Geology, v. 110, pp. 1–000

Gold Behavior in Supergene Profiles Under Changing Redox Conditions: The Example of the Las Cruces Deposit, Iberian Pyrite Belt

Lola Yesares,[1,†] Thomas Aiglsperger,[2] Reinaldo Sáez,[1] Gabriel R. Almodóvar,[1] José Miguel Nieto,[1] Joaquín A. Proenza,[2] Carmelo Gómez,[3] and Juan Manuel Escobar[3]

[1]*Department of Geology, University of Huelva, Avenida de las Fuerzas Armadas, S/N, 21071 Huelva, Spain*

[2]*Departament de Cristal·lografia, Mineralogia i Dipòsits Minerals, Universitat de Barcelona, Martí i Franquès s/n, 08028, Barcelona, Spain*

[3]*Geological Area, Mining Department of Cobre Las Cruces S.A., Gerena, Seville, Spain*

Abstract

The Las Cruces deposit is in the eastern end of the Iberian Pyrite Belt (SW Spain). It is currently being mined by Cobre Las Cruces S.A. The main operation is focused on the supergene Cu-enriched zone (initial reserves of 17.6 Mt @ 6.2% Cu). An Au-Ag-Pb–rich gossan resource (3.6 Mt @ 3.3% Pb, 2.5 g/t Au, and 56.3 g/t Ag) occurs in the upper part of the deposit. The Au grade ranges from 0.01 ppm to >100 ppm, and occurs as three different Au ore types: (1) Au mineralization in the upper part of the gossan linked to Fe-oxides lithofacies, (2) Au concentration in the lower part of the gossan associated with leached black shales, and (3) Au ore in the cementation zone related to subvertical fractures.

A hydroseparation device has been used to obtain heavy mineral concentrates from selected samples of different ore types. Reflected-light microscopy, scanning electron microscopy-energy dispersive spectroscopy (SEM-EDS), and electron probe microanalysis (EPMA) were used to study the separated Au particles. Significant differences between the defined ore types include the Au-bearing lithologies, mineral associations, textural features, particle sizes, morphologies, and fineness. Au-rich minerals include native Au, Au-Ag electrum, and Au-Ag-Hg amalgams. Gold-bearing mineral associations include Pb-oxihalides, Fe-oxides, galena, pyrite, cinnabar, and Ag-sulfosalts.

The Au enrichment mechanism in the supergene profile involves (1) dissolution of Au from the primary sulfides as chloride-rich ionic complexes during the weathering of the deposit under subaerial exposure; dissolved Au is transported downward through the supergene profile under acidic and oxidized conditions; (2) destabilization of the Au complexes by Fe-controlled redox reactions; as a consequence, coarse-grained, high-fineness Au particles precipitated in association with Fe-oxyhydroxides. This resulted in secondary concentration in the upper gossan; and (3) after deposition of cover sediments took place a progressive change in the system conditions resulting in a later Au remobilization as hydroxidehalide, hydroxide, thiosulfate, and bisulfide complexes in the lowermost gossan and cementation zone. The main pathways for migration of enriched fluids to the cementation zone are secondary permeability zones linked to Alpine reactivated faults. Deposition of Au seems to be related to fluid interaction with reductant lithologies, including black shales and the primary sulfides.

Introduction

The study of secondary Au in the weathering environment and the possibility of supergene Au enrichment has been a recurring subject of research (e.g., Boyle, 1979; Webster and Mann, 1984; Stoffregen, 1986; Freyssinet et al., 1989, 2005; Groen et al., 1990; Benedetti and Bouleguè, 1991; Vasconcelos, 1991; Krupp and Weiser, 1992; Bowell, 1993; Gray, 2001; Hough et al., 2008, 2009; Fairbrother et al., 2012; Reith et al., 2012). Secondary Au ores occur mainly as a result of dissolution and redistribution of Au during the weathering of primary sulfides. Supergene Au mobility occurs via complexation with organic-, halide-, hydroxide-, halide-hydroxide and sulfur ligands, which are dependent on weathering conditions (Boyle et al., 1975; Mann, 1984; Webster, 1986, Groen et al., 1990; Benedetti and Bouleguè, 1991; Freyssinet et al., 2005; Tagirov et al., 2006; Usher et al., 2009; Ta et al., 2014). In addition, biological activity can contribute to dissolution-precipitation processes of Au during weathering in the near-surface environment (Reith et al., 2006, 2007, 2012, 2013; Southam et al., 2005, 2009; Hough et al., 2008; Fairbrother et al., 2012).

In general, these processes led to the formation of relatively low grade Au deposits with concentrations ranging between 1 to 5 ppm (Butt, 1998). Secondary Au occurs as fine-grained particles of variable size, in many instances associated with Fe-oxyhydroxide gossans (Mann, 1984; Butt, 1998; Capitan et al., 2003, 2006; Freyssinet et al., 2005; Andreu et al., 2014).

Gossans in the Iberian Pyrite Belt have been mined for Au and Ag since 3000 BC (Nocete et al., 2014) and most supergene Au deposits in the belt, including Riotinto, La Lapilla, and Filón Sur-Tharsis, were mined for precious metals during the past century. The original resources of gossan at Cerro Colorado (Riotinto) exceeded 100 Mt @ 1 g/t Au and 56 g/t Ag, and the gossan at Filón-Sur (Tharsis) contained 15.5 Mt @ 1.7 g/t Au and 29 g/t Ag (Velasco et al., 2013). Previous research on the Iberian Pyrite Belt Au-rich gossans has mainly focused on metallurgy and exploitation of these ores (García Palomero et al., 1986; Viñals et al., 1995; Sánchez et al., 1996; Roca et al., 1999), whereas little attention has been paid to the geologic features and genetic models of this type of weathering-related Au deposit. However, Williams (1950) and Arribas (1998) reported Au-rich ores in Riotinto that mainly occur near the boundary between unweathered massive sulfides and oxidized sulfides, whereas in gossan of Filón-Sur

† Corresponding author: e-mail, lola.yesares@dgeo.uhu.es

Submitted: December 2, 2014
Accepted: June 24, 2015

(Tharsis), the main secondary Au enrichment occurs at intermediate levels associated with goethite (Capitan et al., 2003, 2006). Recently, Velasco et al. (2013) reported that in the gossan deposits of the Iberian Pyrite Belt, there is scarce native free Au, which is very fine grained and of low fineness.

Las Cruces is a currently exploited, volcanic-hosted massive sulfide deposit in the eastern corner of the Iberian Pyrite Belt, about 24 km NW of Seville, Spain. The deposit is mainly characterized by a polymetallic massive sulfide body and by an overlying supergene profile, including the Cu-rich secondary ore (initial reserves of 17.6 Mt @ 6.2 % Cu) and the gossan cap (initial reserves of 3.6 Mt @ 3.3% Pb, 2.5 g/t Au, and 56.3 g/t Ag) (Cobre las Cruces S.A. data calculated on May 11, 2015). The Las Cruces features and genesis have been discussed in recent studies (Knigth, 2000; Capitán, 2006; Blake, 2008; Tornos et al., 2014; Yesares et al., 2014 and 2015), with the main interest focused on the Las Cruces gossan. The most conspicuous irregularities are the lack of an internal structure and an uncommon mineralogy that includes newly formed siderite, Fe-sulfides, galena, and calcite, with goethite and hematite as subordinate phases. Regarding the Las Cruces gossan, the Au distribution has been reported as very heterogeneous, with increasing values toward the lower part of the gossan as supergene Au-Ag-Hg amalgams, mainly associated with reductant lithologies (i.e., black shales and primary sulfides; Yesares et al., 2014).

The present study is the first detailed report of supergene Au mineralization in the Iberian Pyrite Belt. In addition, although little is known about the Au supergene mineralization in this location, the features observed in the supergene Au ore at Las Cruces are inconsistent with those previously reported for the gossans (Williams, 1950; Arribas, 1998; Capitán et al., 2003; Capitán, 2006; Velasco et al., 2013). The main differences lie in Au grade, Au distribution pattern through the supergene profile, Au-bearing lithologies, and size of Au particles and their fineness.

The main objectives of this study were as follows: (1) to determine the distribution of Au and its relationship to the different supergene facies and lithologies, (2) to describe the mineralogical and textural features of the different Au ores, (3) to characterize the chemical make-up of the different Au particles, (4) to identify the possible mechanisms of Au transport and precipitation in the supergene profile, and (5) to report on the new insights of genetic models dealing with the supergene mineralization of Las Cruces.

Methods

Samples were collected from both open pit outcrops (samples weighing >1 kg) and drill core (sample length ≈ 1 m) throughout the different facies of the Las Cruces supergene profile. Samples were processed as follows.

1. Bulk geochemical analysis of 48 whole-rock samples was performed at Acme Analytical Laboratories LTD (Vancouver, Canada). The major, minor, and trace element contents (including Au) were determined by inductively coupled plasma optical emission spectrometry (ICP-OES) and inductively coupled plasma-mass spectrometry (ICP-MS) after hot aqua regia digestion (95°C). To carry out the analysis, certified standard reference materials and quartz blanks were routinely prepared and analyzed in the same way as the supergene profile samples. Only Au results have been considered for this paper.

2. Three Au samples assaying >100 ppm Au were selected and sent to the hydroseparation laboratory in Barcelona (www.hslab-barcelona.com) to obtain heavy mineral concentrates. A total of 43 g from the Fe-oxide facies, 505 g from the leached black shales horizon, and 67 g from the cementation zone were roughly disaggregated with an agate mortar and dispersed in water by means of an ultrasonic bath. The sample slurries were subsequently wet sieved through a standard screen series, resulting in the size fraction distribution given in Table 1. Heavy mineral concentrates of each size fraction were processed by using the computer-controlled device CNT HS 11 (Rudashevsky et al., 2001; Rudashevsky and Rudashevsky, 2006, 2007; <http://www.cnt-mc.ru/>). Details about the applied hydroseparation technique can be found in Aiglsperger et al. (2014, and references therein).

3. Four cylindrical monolayer polished sections (2.5 cm diam) were prepared from each final concentrate. Au textures, mineral associations, and grain sizes were examined by reflected light optical microscope.

4. Electron-probe microanalysis (EPMA) of Au particles was carried out on carbon-coated samples with a JEOL JXA-8200 Super Probe Electron Probe Micro-Analyzer by wavelength-dispersive spectroscopy (WDS) at the University of Huelva (operated at 20 kV, 20 nA, and 5–10-μm beam diam). A total of 142 Au grains (polished sections) were analyzed for Au, Ag, Cu, Sb, Fe, Se, Pb, S, and Hg. Routine data reductions, including full matrix (ZAF) corrections, were performed. Core and rim compositions of Au grains were obtained to investigate possible Au zonation.

5. Several Au grains found in heavy mineral concentrates from the gossan were handpicked under a binocular microscope and mounted on glass slides with double-sided adhesive tape for grain morphology studies. A JEOL scanning electron microscopy-energy dispersive spectroscopy (SEM-EDS) was used at the University of Huelva.

Geologic Setting

The Iberian Pyrite Belt is in the southwest part of the Iberian Peninsula and is about 230 km long and 40 km wide, extending from Seville (Spain) to Lisbon (Portugal) (Fig. 1). The Iberian Pyrite Belt is one of three domains making up the South Portuguese zone, which is the southernmost zone of the Iberian Variscan Massif (Carvalho, 1976). The Iberian Pyrite Belt is recognized as one of the most prolific massive sulfide provinces in the world (Leistel et al., 1998; Sáez et

TABLE 1. Weight and Size Fraction Distribution of the Heavy Mineral Concentrates

Size (μm)	Fe-oxide facies (wt gr)	Leached black shales (wt gr)	Cementation zone (wt gr)
>53	35.3	386.6	15.0
53	0.4	56.4	16.3
75	1.9	62.5	20.1
106	5.1	-	14.2
<125	0.3	-	1.5
Σ wt gr	43.0	505.5	67.1

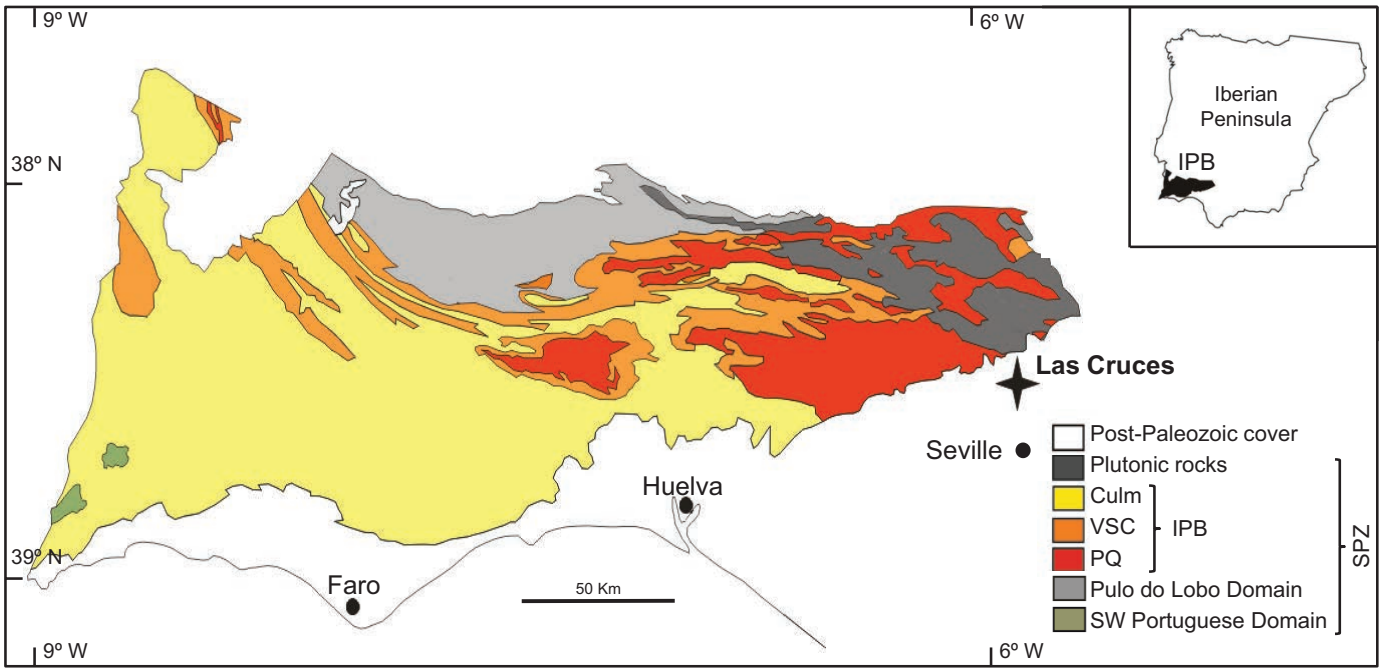

FIG. 1. Geologic map of the South Portuguese zone showing the location of the Las Cruces deposit in the southeastern part of the Iberian Pyrite Belt (modified from Carvalho, 1976). Abbreviations: IPB = Iberian Pyrite Belt, PQ = phyllite-quartzite group, VSC = volcano-sedimentary complex, Culm = Culm Group, SPZ = South Portuguese zone.

al., 1999). It consists of upper Paleozoic (Middle Devonian to Middle Pennsylvanian) sedimentary and igneous rocks, which include, from bottom to top, three main units: (1) the Givetian-Famennian prevolcanic phyllite-quartzite group; (2) the late Famennian-Tournaisian volcano-sedimentary complex; and (3) the middle Visean-Westphalian B post-volcanic Culm Group (Schermerhorn, 1971). The massive sulfide deposits of the Iberian Pyrite Belt occur within the volcano-sedimentary complex associated mainly with volcaniclastic and/or black shale sequences. Deformation during the upper Carboniferous was a thin-skinned style (Silva et al., 1990) characterized by stacking of tectonic slices, folding, and very low grade metamorphism. Exhumation of some massive sulfide deposits during the lower Miocene led to weathering and the formation of gossan caps (Essalhi et al., 2011; Velasco et al., 2013). Later, the Miocene transgression event (Abad, 2007) buried parts of the Iberian Pyrite Belt under post-Alpine sediments of the Guadalquivir (Spain) and Sado (Portugal) basins.

Deposit Geology

The Las Cruces deposit is in the eastern end of the Iberian Pyrite Belt and lies under a thick sequence (140–150 m) of carbonate-rich, detrital sedimentary cover of the post-Alpine (Neogene-Quaternary) Guadalquivir basin (Fig. 1). The Las Cruces deposit is hosted by a thick sequence of black shales and felsic volcanic and volcaniclastic rocks and consists of a massive to semimassive polymetallic sulfide body that is underlain by a copper-rich pyritic stockwork (Fig. 2). The orebody is approximately 60- to 100-m thick and extends for more than 1 km in an east-west direction, dipping 35° to the north. The upper part of the massive sulfide consists of a supergene profile that includes a copper-rich cementation zone and an overlying gossan.

The Las Cruces orebody structures are consistent with the tectonic setting established for the Iberian Pyrite Belt by Silva et al. (1990). Three structural domains have been observed at the deposit scale. The first fault system includes low-angle faults associated with the first Variscan deformation. This fault system was responsible for shearing of the orebody and resulted in stacking of massive sulfide slices. Sheared black shale horizons appear to play a major role as detachment horizons. Las Cruces is crosscut by two other subvertical fault systems related to the late-Variscan deformation, as reported for others areas of the Iberian Pyrite Belt (Simancas, 1983). The older system consists of NNW-SSE–trending faults that are intersected by a younger system of east-west, high angle faults. Both late-Variscan fault systems were reactivated during the Alpine cycle and contributed to secondary enrichment processes.

The primary sulfides at the Las Cruces deposit are similar to other massive sulfide deposits in the Iberian Pyrite Belt (García de Miguel, 1990; Marcoux et al., 1996; Almodóvar et al., 1998) and consist of pyrite, with subordinate amounts of chalcopyrite, sphalerite, and galena. Tennantite-tetrahedrite, arsenopyrite, and several Bi and Pb-sulfosalts are mostly present as accessory minerals. The ore, however, is very irregular in shape and mineralogy and includes barren pyrite and polymetallic- and copper-rich facies.

Supergene profile

The upper part of the orebody is largely replaced by a thick supergene profile that includes the gossan and the underlying cementation zone. The cementation zone consists of a

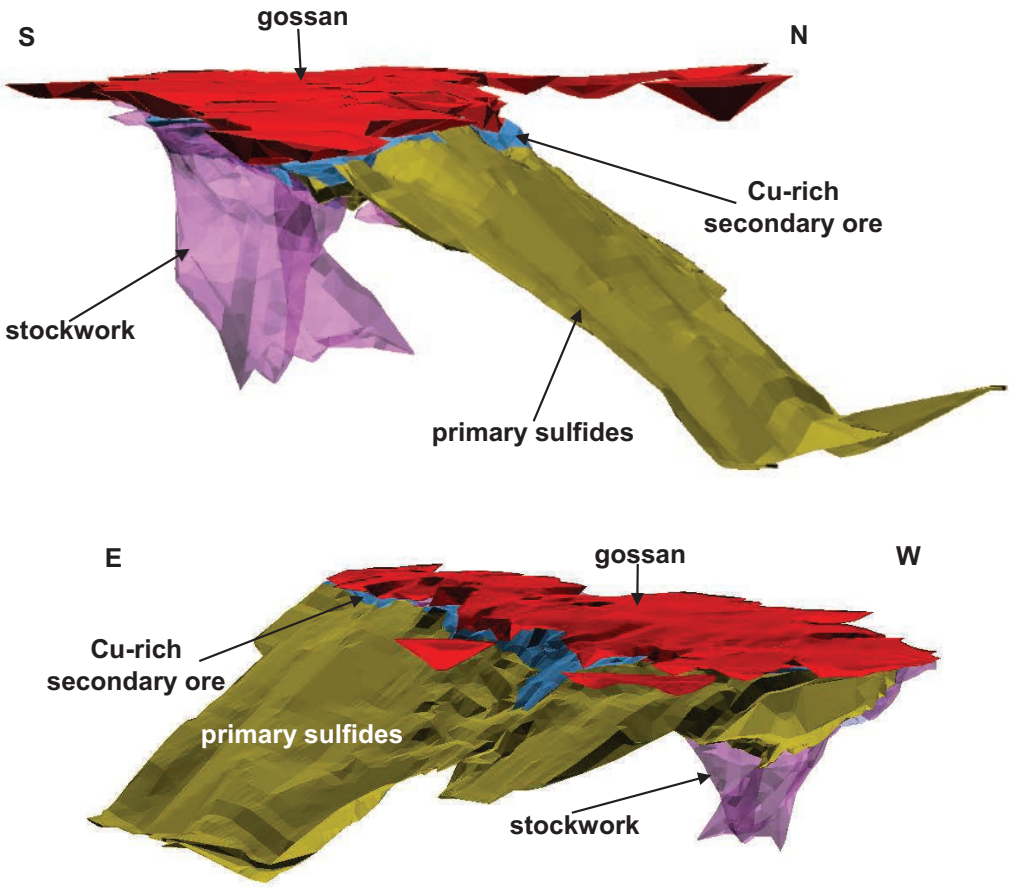

FIG. 2. Geologic cross section of the Las Cruces deposit.

50-m-thick lens that is mostly developed through higher permeability zones associated with late-Variscan subvertical faults (Yesares et al., 2014, 2015). Several facies have been identified along the cementation zone by mineralogical features:

1. *Pyritic sands:* This facies is at the top of the cementation zone and consists of a 0- to 5-m-thick layer of sand-like (crumbled and leached) barren pyrite;
2. *Chalcocite-rich secondary ore:* This facies underlies the pyritic sands and represents the main Cu supergene enrichment of the primary sulfides, both massive sulfides and stockwork mineralization. The mineral assemblage mostly consists of chalcocite, digenite, and djurleite, with minor covellite, bornite, and enargite;
3. *Covellite-rich secondary ore:* This is a 12-m-thick body at the base of the cementation zone, which is developed throughout a deep subhorizontal fault. It mainly consists of covellite with minor chalcocite, digenite, enargite, and bornite;
4. *Fault breccia-related Au-Ag–rich secondary ore:* This facies consists of a 0- to 5-m-wide subvertical fault-breccia zone that crosscuts the cementation zone. It contains coarse-grained proustite, pyrargyrite, cinnabar, and native Au.

The gossan mineralization consists of a 0- to 20-m-thick profile that is limited at the base by a sharp horizontal contact with the massive sulfides. The upper boundary of the gossan is defined by the erosive discordance of the Guadalquivir basin sedimentary cover. The occurrence of gossan pebbles within the overlying conglomerate level in the sedimentary cover indicates that the supergene process in Las Cruces deposit predates the transgressive Tortonian deposits (Moreno et al., 2002).

Yesares et al. (2014, 2015) concluded that the Las Cruces gossan differs from other massive sulfide weathering profiles in tonnage, grade, zonation, and internal structure. The most conspicuous feature, however, is its mineralogical composition. The major mineral components of the gossan are reduced iron phases such as siderite and Fe-sulfides, together with galena and calcite, whereas goethite and hematite are subordinate phases. Four facies have been identified within the Las Cruces gossan:

1. *Carbonate-sulfide facies:* These are the main gossan facies and are heterogeneously distributed throughout the profile and controlled by subvertical faults. The mineral assemblage consists of siderite, calcite, galena, and Fe-sulfides, with minor hematite and goethite and subordinate Ag-sulfides and Au-Ag-Hg amalgams;
2. *Fe-oxide facies:* These are typically close to highly permeable zones and are composed of siderite, Fe-sulfides, and galena, with minor goethite and hematite;
3. *Fracture-related facies:* These consist of siderite, calcite, galena, and Fe-sulfides. This assemblage fills late fractures that crosscut the gossan;

4. *Leached black shales:* These consist of a 5- to 15-cm-thick horizon located at the gossan bottom. This black shale level has been interpreted as a low-angle Variscan fault detachment slice that acted as a redox front during weathering (Yesares et al., 2014). It consists of an assemblage of residual minerals such as quartz, barite, monazite, Ti-oxides, newly formed phyllosilicates of the smectite and kaolinite groups, galena, Ag-sulfides, cinnabar, and Au-Ag-Hg amalgams.

Results

Au distribution in the supergene profile

Au concentrations in the primary sulfides of the Las Cruces deposit are mainly associated with polymetallic mineralization with average values of 0.7 ppm, whereas gossan has an Au mean value of 5.88 ppm (Yesares et al., 2014, 2015). Gold concentrations are highly variable throughout the gossan but the overall enrichment ratio relative to the primary mineralization is 8.4. The highest Au concentrations occur close to the gossan base associated with Au-Ag-Hg amalgams. Several peak Au values, however, are in the upper part of the weathering profile associated with particulate Au.

The Au contents of selected samples from the different supergene facies are presented in Table 2. Gold distribution in the different supergene facies is extremely heterogeneous, ranging from 0.01 to >100 ppm. In the gossan, Au is mainly associated with both Fe-oxide facies and leached black shales, and minor amounts have been analyzed in carbonate-sulfide facies. In Fe-oxide facies and black shales, Au reaches more than 100 ppm (the upper detection limit for ICP assays) and has mean values of 20 and 36 ppm, respectively, whereas the carbonate-sulfide facies has an Au mean concentration of 1.66 ppm, ranging from 0.01 to 9 ppm. Gold distribution also shows a strong heterogeneity within the cementation zone. The Au content in the supergene Cu-rich mineralization is generally low, ranging between 0.03 and 0.77 ppm. Local peak values of up to 100 ppm are systematically associated with subvertical faults that mainly controlled the secondary mineralization processes.

TABLE 2. Gold Content (ppm) of Selected Samples from Las Cruces Gossan Based on ICP Analysis

Sample no.	Carbonate-sulfide facies	Fe-oxide facies	Leached black shales	Cementation zone
1	1.64	>100.00	40.15	0.03
2	1.02	6.47	60.84	0.09
3	9.64	0.96	2.42	0.30
4	1.22	0.17	0.58	0.08
5	1.67	0.51	0.62	0.07
6	4.00	2.64	83.13	0.04
7	1.61	0.26	>100.00	>100.00
8	0.21	0.24	2.60	0.77
9	1.29	89.77		0.35
10	0.56	0.17		0.10
11	0.71			0.56
12	0.37			
13	1.74			
14	0.19			
5	0.01			
16	0.45			
17	4.95			
18	0.02			
19	0.16			
Mean	1.66	20.12	36.29	9.31
Max	9.64	>100.00	>100.00	>100.00
Min	0.01	0.17	0.58	0.03
Std. dev.	2.33	39.53	40.88	30.08

Basic statistical parameters—mean, maximum (Max), minimum (Min), and standard deviation (Std. dev.)—are shown

The most common mineral association in Fe-oxide facies consists of goethite, hematite, and minor siderite, pyrite, and galena. Common textures include goethite and hematite as slightly rounded isolated fragments enclosed in later microcrystalline siderite, and alternating microlayers of goethite and siderite (Yesares et al., 2015; Fig. 3A). Both textural patterns include pervasively disseminated Au particles (Fig. 3A-F).

The principal mineral associations in the fault breccia-related Au-Ag–rich secondary ore in the cementation zone are composed of fault gouge mainly formed by pyrite clasts and newly formed cinnabar, pyrargyrite, proustite, and native Au. The most prominent textures are coarse-grained euhedral-anhedral aggregates of Ag-sulfosalts and cinnabar filling fractures and voids (Fig. 4A, B). Gold occurs as disseminated free grains (Fig. 4D-F).

Size and morphology of Au grains

The gold grains from the Las Cruces Fe-oxide supergene facies include a wide variety of morphologies. Three Au subtypes have been identified based on their morphology. The largest subtype consists of irregular, reniform particles of 100- to 250-μm-diameter (maximum dimension). These particles are anhedral in habit and have smooth-curved and twisted surface sides and rounded edges (Figs. 3D, 5A). A second Au subtype occurs as flattened particles with grain sizes ranging from 25 to 150 μm in long axis. These platelet Au grains have a subhedral habit and flat surfaces, jagged contours, and sharp edges (Fig. 5B). The third Au subtype is characterized by round to subround-shaped grains of 50- to 150-μm long axis diameter. These particles have irregular surfaces, straight sides, and subrounded edges (Fig. 5C). In addition, some of the Au particles observed in polished sections exhibit crystal faces (Fig. 3C).

Most of the Au particles occur as free grains (Figs. 3, 5). Moreover, Au occurs in complex relationships with other gossan minerals such as the case of elongated Au crystals (>50 μm in length) associated with galena (Fig. 3E) or fine Au (<20 μm diam) associated with nadorite (Fig. 3F).

Secondary Au mineral associations in the fault breccia-related Ag-Au–rich secondary ore in the cementation zone consist mainly of free Au particles with grain sizes varying from a few microns to 70 μm in maximum dimension. Au grains exhibit anhedral habit, with regular and subrounded to rounded morphologies (Fig. 4D-F). Gold usually presents as intergrowth relationships with proustite (Fig. 4F), whereas cinnabar occurs as small inclusions within Au (Fig. 4E).

Gold chemistry

EPMA analyses of different Au ore types reveal a remarkable compositional variation (Table 3). Figures 6 and 7 show the Au-Ag-Hg ratio and the Au trace element contents of different ore types. The composition of the Au-Ag-Hg system indicates two compositional trends: one is associated with

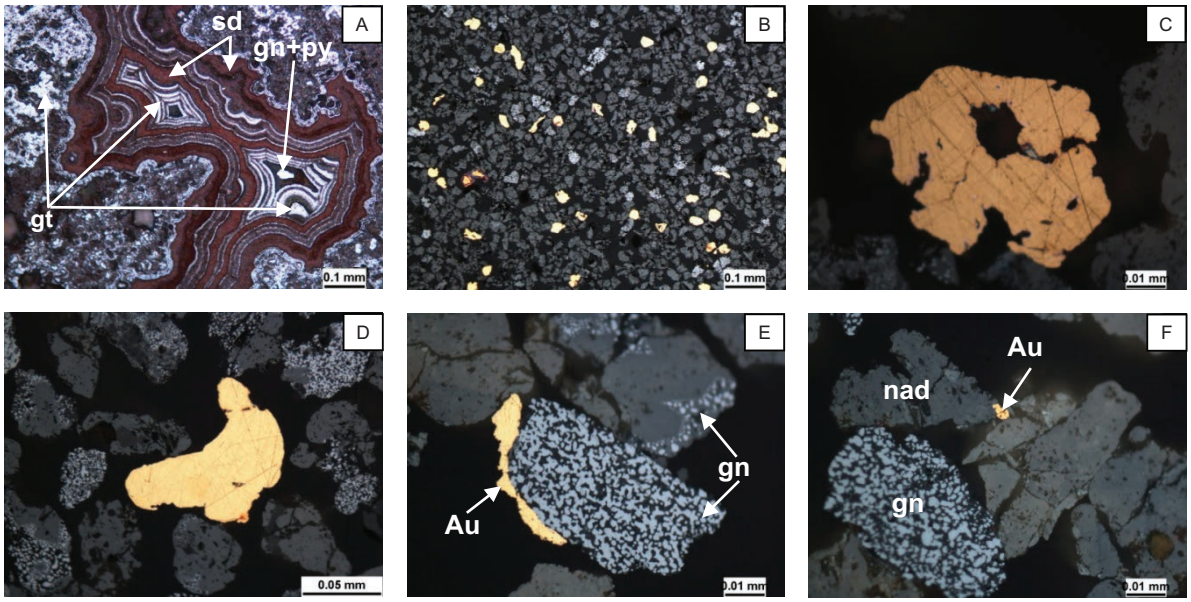

FIG. 3. Reflected light microscopy images of the Las Cruces supergene Au from the upper gossan Fe-oxide facies. (A) Microbanded texture of alternating siderite (sd) and goethite (gt), with galena (gn) and pyrite (py) filling voids; (B) Microscopic appearance of the <53-μm fraction of heavy-concentrates; (C) Detail of the free Au particles showing euhedral-to-subhedral habits; (D) Lobular-shaped free Au grains; (E) Elongated Au (Au) crystals associated with skeletal galena (gn); (F) Fine Au (Au) particles linked to microcrystalline nadorite (nad).

Fe-oxides facies whereas the other is associated with fault breccias in the cementation zone. Figures 6 and 7 also illustrate a third Au compositional cluster, formed by Au-Ag-Hg amalgams in lower gossan formed in leached black shales (Yesares et al., 2014).

Gold associated with Fe-oxide facies has a homogeneous composition (Table 3; Figs. 6, 7) without compositional zonation. Grains exhibit a mean Au content of 99 wt %, low concentrations of commonly alloyed elements (Table 3: 0.09 ± 0.19 wt % Ag, 0.06 ± 0.01 wt % Cu, and 0.006 ± 0.03 wt % Hg), and exceedingly high fineness (1,000 Au/Au + Ag) reaching up to 1,000. The content of trace elements typically present in native Au including Sb, Fe, Se, and Pb are close to or below the limit of detection for EPMA analyses (Table 3). On the other hand, significant sulfur has consistently been detected, with mean values of 0.059 wt %.

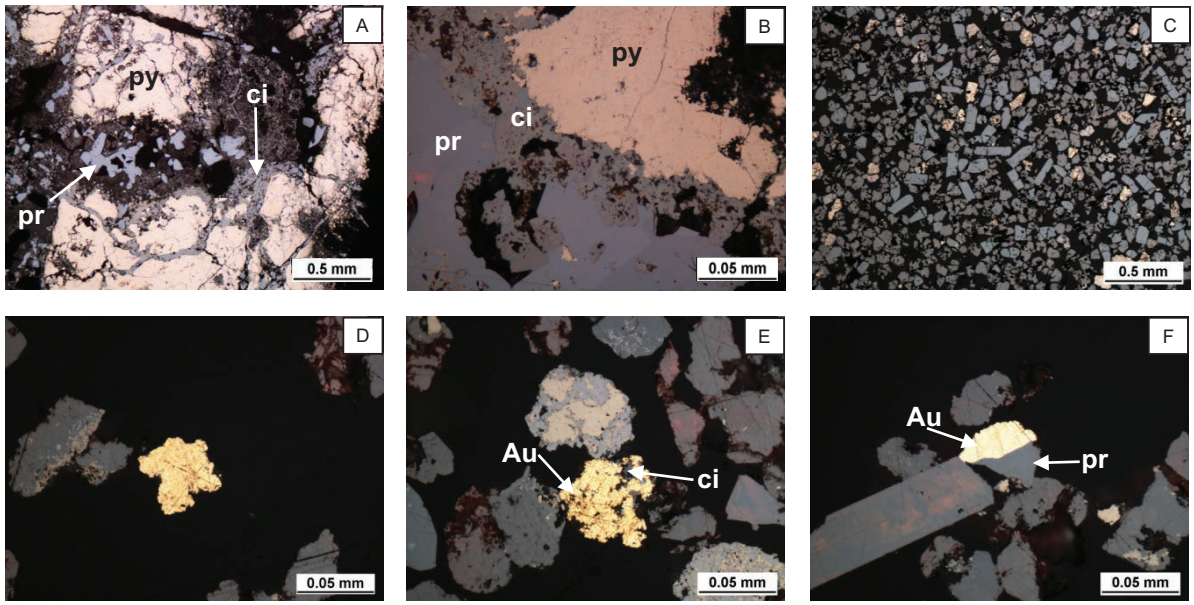

FIG. 4. Reflected light microscopy images of the Las Cruces supergene Au from breccia-related Au-Ag-rich secondary ore located in the cementation zone. (A, B) Cinnabar (ci) and proustite (pr) intergrowth filling fractures in brecciated pyrite (py) fault gouge; (C) polished section microscopic appearance of the 53 μm heavy-concentrates; (D) detail of common shapes of free Au particles; (E) irregular Au (Au) grain with cinnabar (ci) inclusions; (F) intergrowth between proustite (pr) and Au (Au).

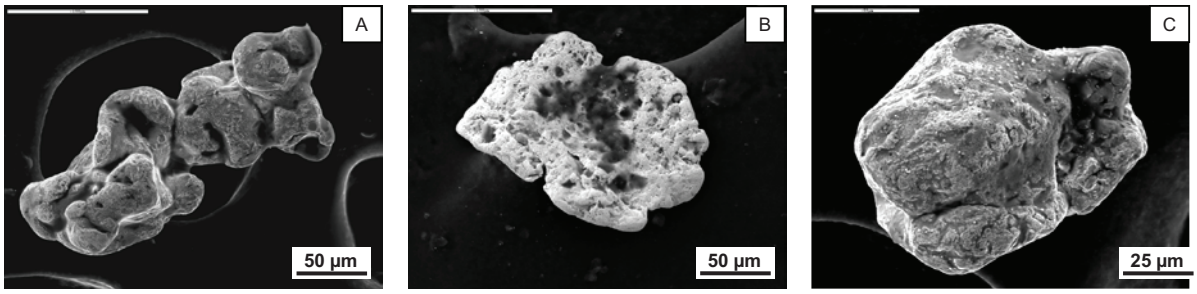

FIG. 5. SEM images showing morphological features of the Las Cruces supergene Au from the upper gossan Fe-oxide facies. (A) Reniform-shaped Au grains showing smooth curved and twisted surface sides and round edges; (B) Flattened Au particles which exhibit euhedral-to-subhedral habit, flat surfaces, and sharply defined edges; and (C) round to sub-round shaped Au showing irregular surfaces, straight sides, and subrounded edges.

In contrast, Au associated with fault breccias within the cementation zone is characterized by wider compositional variations (Table 3; Figs. 6, 7). Gold content for this ore type ranges from 65.3 to 88.9 wt %, with fineness grades ranging from 722 to 948. No zonation has been observed in SEM backscattered studies. Gold grains are relatively rich in commonly alloyed elements: 17.79 ± 5.99 wt % Ag, 0.02 ± 0.02 wt % Cu, and 4.46 ± 2.64 wt % Hg (Table 3; Figs. 6, 7). Trace element contents are close to or below the limit of detection (Table 3), and as with Au associated with Fe-oxide facies, S is the most abundant trace element, with average values of ~0.17 wt %. Neither Au or Au-Ag-Hg amalgam particles have been found in heavy mineral concentrates from the leached black shale samples.

Discussion

Three main types of Au-bearing mineralization occur in the Las Cruces supergene profile. Differentiation is based on Au geochemistry, depositional context, and supergene traps, mineral associations, Au textures (crystal morphology and grain size), and fineness, including the following:

1. Coarse grains of high-fineness Au in the Fe-oxide facies of the upper gossan (Figs. 3, 5, 7, 8; Tables 2, 3);
2. Coarse Au-Ag-Hg amalgams in the lower gossan associated with leached black shales (Yesares et al. 2014);
3. Medium-sized Au particles of medium fineness in fault breccia-related Au-Ag–rich secondary ore in the cementation zone (Fig. 4; Tables 2, 3).

During economic evaluation of the Las Cruces deposit Cobre las Cruces S.A. did not discriminate among the different gossan lithologies. However, observations during mining operations revealed that replacement of the original gossan by carbonate-sulfide facies (siderite-sulfides facies + calcite-sulfide facies) was mainly controlled by subvertical faults; a considerable part of the weathering profile was unaffected by the carbonatization processes. The remnants of the original weathering profile include the Fe-oxide facies and leached black shales. These units have high gold grades (Table 2), thus proving that carbonatization processes were not the main factor for Au concentration in the Las Cruces gossan. This contradicts the interpretation of Tornos et al. (2014), which equated Au with the calcite-rich lithologies in the supergene profile.

All these Au ore types identified in the Las Cruces supergene profile are related to Au leaching from the primary mineralization and precipitation both in gossan and cementation zones. The high-fineness Au particles identified in the upper gossan are consistent with secondary Au enrichment described in mature weathering environments (Mann, 1984; Butt, 1998; Gray et al., 1992; Freyssinet et al., 2005), which can generally be differentiated from hypogene Au-Ag alloys (Boyle, 1979; Hough et al., 2009). According with Au compositions reported in IPB primary massive sulfides (Fig. 8; Leistel et al., 1998; Velasco et al., 1999; Pinto et al., 2005; Oliveira et al., 2011), the Las Cruces gossan high-fineness Au can be interpreted to result from a chemical refining process during

TABLE 3. EPMA Analysis of Gold Ore Types in the Las Cruces Supergene Profile

Gold type	(wt %)	Au	Ag	Cu	Sb	Fe	Se	Pb	S	Hg	Total	Fineness
Gold from Fe-oxide facies of the upper gossan												
(*n* = 133)	Mean	99.03	0.09	0.00	0.02	0.00	0.01	0.01	0.05	0.00	99.23	999.05
	Max	100.55	1.32	0.09	0.21	0.11	0.07	0.16	0.15	0.30	100.74	1000.00
	Min	92.55	n.d	n.d	n.d	n.d	n.d	n.d	0.02	n.d	93.61	986.64
	Std. Dev.	0.97	0.19	0.01	0.05	0.01	0.01	0.03	0.02	0.03	0.92	2.00
Gold from breccia-related Au-Ag-rich secondary ore of the cementation zone												
(*n* = 9)	Mean	76.62	17.79	0.02	0.02	0.03	0.07	0.02	0.17	4.46	99.17	810.68
	Max	88.91	25.15	0.06	0.10	0.10	0.31	0.15	0.63	8.35	100.55	948.15
	Min	65.30	4.86	n.d	n.d	n.d	0.00	n.d	0.07	1.59	97.04	721.89
	Std. dev.	7.54	5.99	0.02	0.03	0.03	0.10	0.05	0.17	2.64	0.95	67.05

Notes: Basic statistic parameters—mean, maximum (Max), minimum (Min), and standard deviation (Std. dev.)—are shown; n.d.: not detected

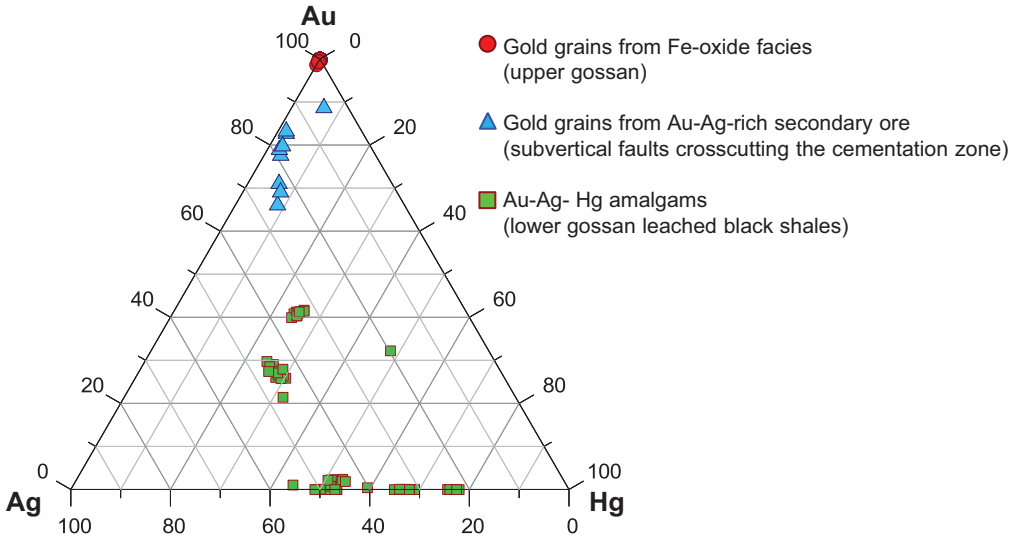

FIG. 6. Composition of Au grains in the Au-Ag-Hg ternary diagram. Three clusters can be distinguished according to elemental ratios. A fourth cluster Ag-Hg amalgams is depicted close to the lower axis. Amalgam compositions from Yesares et al. (2014).

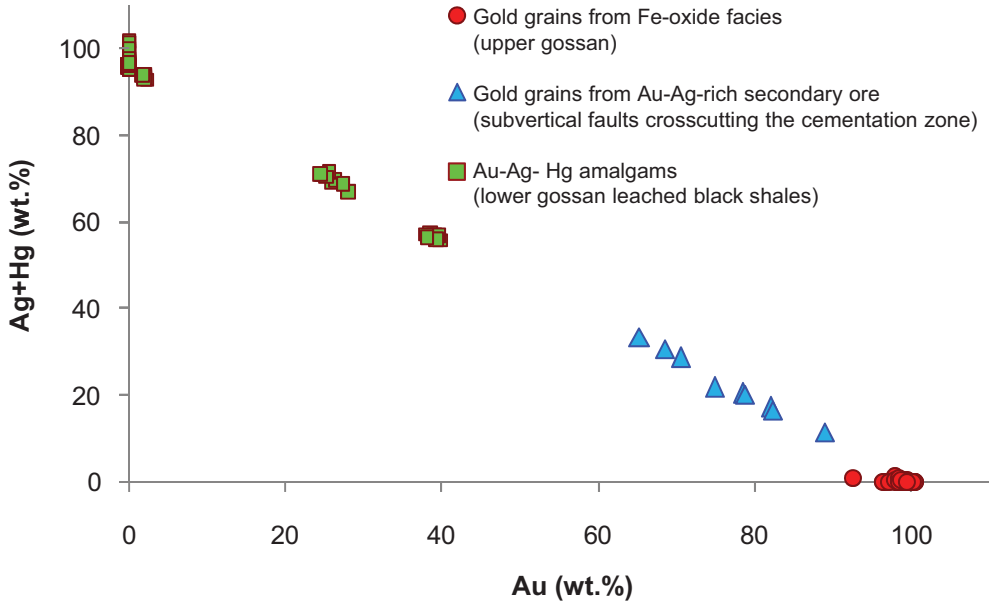

FIG. 7. Ag + Hg vs. Au diagram showing the main chemical composition of the Las Cruces supergene Au grains, based on EPMA analysis. Amalgam compositions from Yesares et al. (2014).

the weathering and dissolution of primary Au and reprecipitation as newly formed Au particles (Mann, 1984; Williams et al., 2009; Hough et al., 2011).. Likewise, trace elements such as Sb, Fe, Se, Pb, and S in Au grains (Table 3) seem to be derived from micro-inclusions of common minerals in the Las Cruces gossan, such as galena, Pb-Sb-sulfosalts, siderite, Fe-oxides, and Fe-sulfides (Yesares et al., 2014, 2015). Textural features of Au grains (smooth surfaces) and the lack of zonation of Au and Ag within the particles suggests that dealloying processes do not increase the fineness of Au particles (Erlebacher et al., 2001; Hough et al., 2007). The high fineness of Au particles in the Las Cruces gossan contrasts with the relatively low fineness of Au particles reported in other Iberian Pyrite Belt gossans (Velasco et al., 2013).

Medium fineness Au particles are also consistent with a newly-formed phase due to their specific location (Fig. 9) and their mineral associations (Fig. 4). These medium fineness Au grains are closely linked to supergene proustite and cinnabar, which are common in late-subvertical faults gouge, crosscutting the Las Cruces cementation zone. These structures exert a significant control on the distribution of the secondary mineralization and its role in the supergene enrichment process has been discussed by Yesares et al. (2014, 2015) (Fig. 9). Furthermore, Au-Ag-Hg amalgams in the lower gossan show

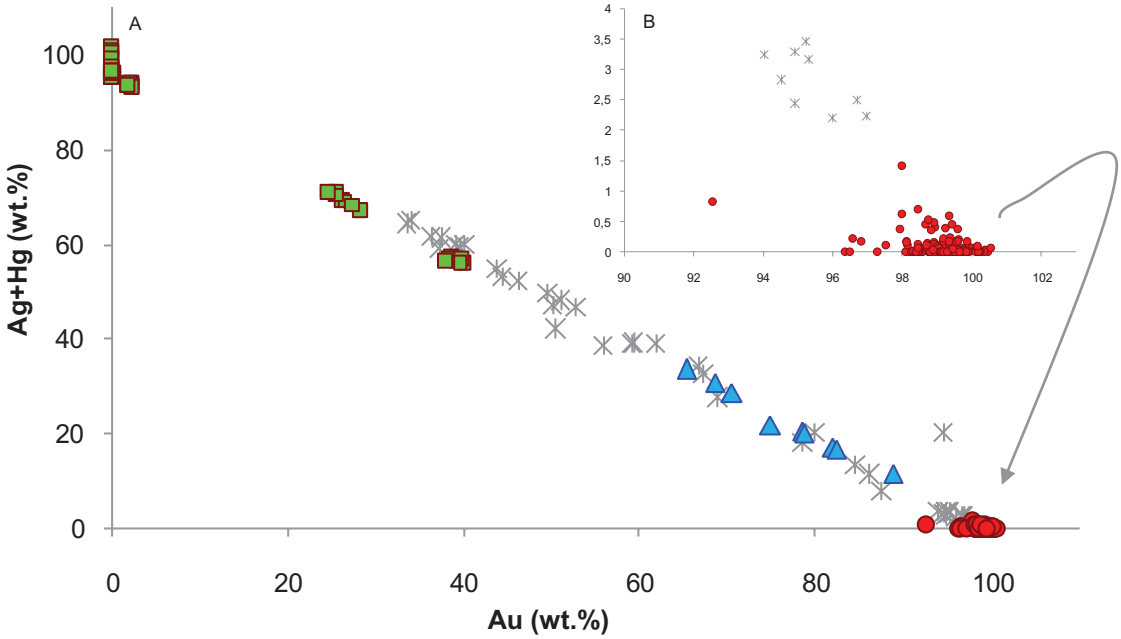

FIG. 8. Ag + Hg vs. Au diagram contrasting the composition of the Las Cruces supergene Au grains with Au from Iberian Pyrite Belt unaltered massive sulfides (Leistel et al., 1998; Velasco et al., 1999; Pinto et al., 2005; Oliveira et al., 2011).

also textural evidences for supergene deposition (Yesares et al, 2014).

The existence of three different Au ore types in the supergene profile has implications for Au mobilization and precipitation mechanisms including:

1. The presence of different Au composition types in the Las Cruces supergene profile (Table 3; Figs. 6, 7) suggests that more than one mechanism could have been involved in Au dissolution and mobilization during the weathering of sulfide ores and the later evolution during subsequent sedimentation (Fig. 9);
2. The Au distribution is not uniform throughout the supergene profile, thus indicating multiple fluid pathways (Fig. 9);
3. Each Au type is intimately associated with a specific supergene facies, involving different lithologic traps and precipitation mechanisms (Fig. 9).

The overall supergene profile is the result of overlapping genetic stages, including oxidative weathering of the massive sulfide during deposit exhumation, as well as changes in redox conditions during the later burial of the deposit beneath the Neogene sedimentary cover (Fig. 9). Thus, the environmental conditions of gossan formation changed from oxidizing and acidic during the early stage of gossan formation upon surface exposure, to near-neutral and reducing during the burial stage due to basinal fluid equilibration with the carbonate-rich sedimentary pile. (Fig. 9)

The uneven Au distribution within the Las Cruces gossan and its enrichment toward the lower gossan is a common feature in weathering profiles of a VMS deposit (e.g., Zapdno-Ozeroe, South Urals (Belogub et al., 2003); and TAG and Cyprus Troodos Ophiolite (Herzig et al., 1991), including those in the Iberian Pyrite Belt gossans (Williams, 1950, Arribas, 1998; Velasco et al., 2013). However, Au concentration for the Las Cruces gossan (greater than 100 ppm) is higher than for other Iberian Pyrite Belt gossans (0.02–10.49 ppm Au, Velasco et al., 2013). In addition, the distribution of Au in the cementation zone of Las Cruces differs from that described in other supergene profiles. Both the high Au concentration and the dispersion patterns in the Las Cruces supergene profile suggest that the metals have been remobilized and subsequently precipitated by a wide range of mechanisms as has been proposed for other supergene profiles (Mann, 1984; Webster and Mann, 1984; Gray et al., 1992; Butt, 1998; Freyssinet et al., 2005; Capitán, 2006; Reith et al., 2007; Williams et al., 2009; Andreu et al., 2014).

The fineness of secondary Au in a supergene profile can be attributed to the ligands that are responsible for Au migration after its dissolution (Gray et al., 1992; Freyssinet et al., 2005). In this way, high-fineness Au located within the Fe-oxides facies in the upper gossan (Figs. 3, 5–8; Tables 2, 3) results from Au-chemical refining (Fig. 8), which is produced by precious metal mobilization during oxidation of the primary ores via halide-complexes in acidic, Fe-rich, oxygenated, and saline conditions (Mann, 1984; Gray et al., 1992; Saunders, 1993; Butt, 1998; Gray, 2001; Freyssinet et al., 2005).

This stage coincides with the early Miocene exhumation and oxidation of the Las Cruces deposit (Fig. 9). In addition to the acidic, Fe-rich, and oxygenated conditions that characterize the supergene environment, the closeness of the seashore (Martín-Algarra and Vera, 2004) during this period could have provided enough sea aerosols to supply Cl, I, and Br in the Las Cruces weathering environment. The stratigraphic record of the Las Cruces area indicates a marine incursion during Miocene times (Abad, 2007; Pérez-Asensio et al., 2014) and, as a result, the Las Cruces deposit was subject to pervasive seawater-gossan interaction (Yesares et al., 2015). Nadorite ($PbSbO_2Cl$) has been identified as a common phase in close

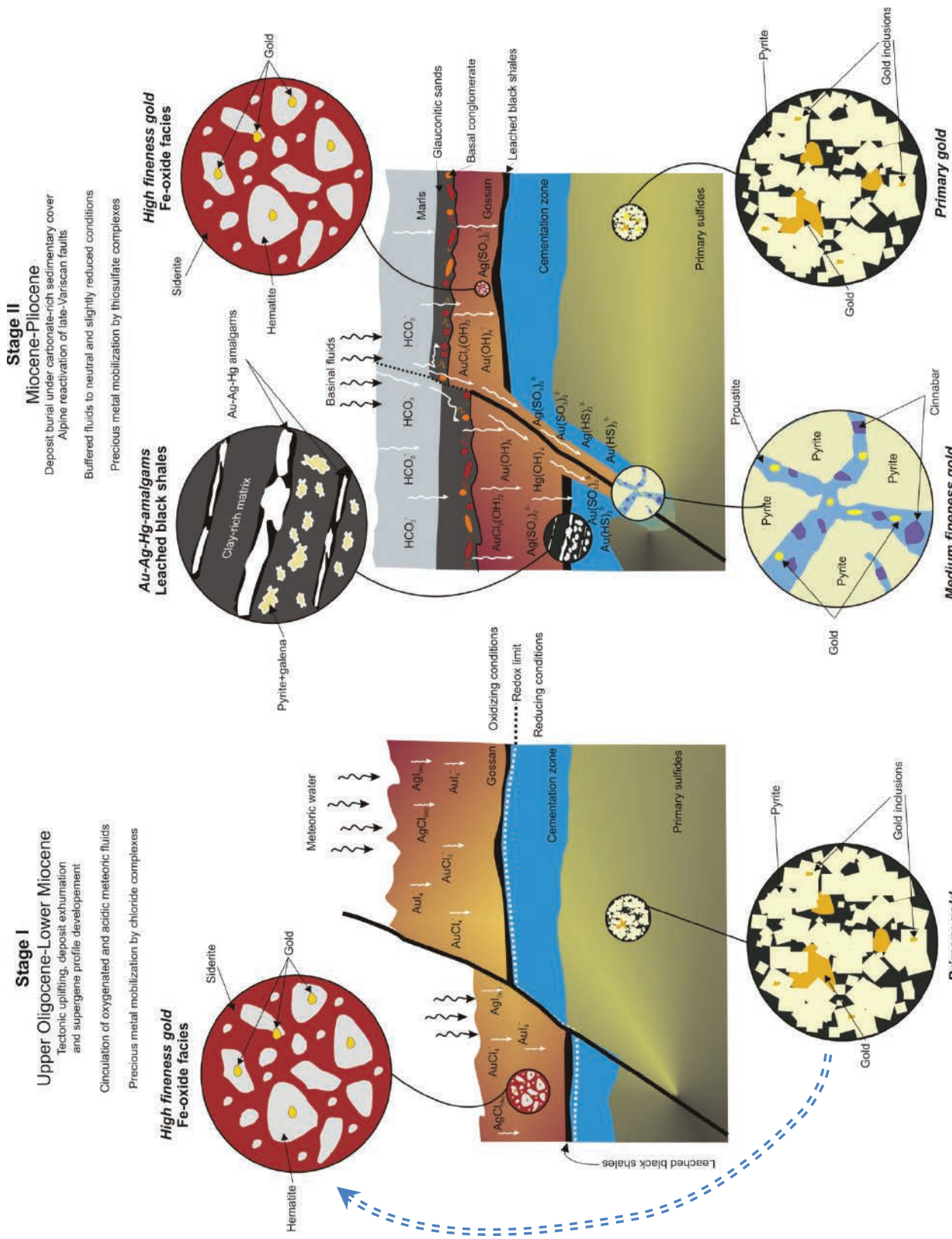

FIG. 9. Two-stage genetic model for the Las Cruces Au mineralization. Stage 1. Precious metals mobilization and fixation during weathering of the massive sulfide deposit and gossan and supergene profile development. Stage 2. Later supergene profile evolution beneath the carbonate-rich sedimentary cover. See text for explanation.

association with Au particles in the Fe-oxides facies in the Las Cruces gossan and may reflect saline seawater involvement (Fig. 3F).

Au mobilization in Cl-rich systems has been discussed by Usher et al. (2009) who reported halide Au-complexes as the main soluble Au species in oxidized waters at 25°C. These include $(AuCl/Br_4)^-$ at <4 pH, $(AuOH_4)^-$ at <10 pH, and hydroxidehalide-mixed complexes at intermediate pH conditions. Ta et al. (2014) reported such Au^{3+}-halidehydroxide complexes in natural hypersaline waters.

Marine aerosol involvement in the formation of Au-halide or Au-hydroxidehalide complexes is supported also by the fact that other Iberian Pyrite Belt gossans contain iodargyrite and chlorargyrite as the main Ag-bearing minerals (Capitán, 2006; Velasco et al., 2013), especially in deposits which were closer to the sea during the Miocene marine transgression (e.g., Filón Sur-Tharsis). The precipitation of these Ag-halides phases results in the fractionation of Au/Ag in Cl-rich systems (Mann, 1984; Krupp and Weiser, 1992; Saunders, 1993). Furthermore, Ag-halides are commonly interpreted as indicators of extremely arid environments (Boyle, 1997; Reich et al., 2009; Golebiowska et al., 2010; Velasco et al., 2013), although Ag-halides have also recently been described in a tropical developed gossan by Andreu et al. (2014).

Medium-fineness Au located in the gossan base and in fault breccias in the cementation zone is related to the later evolution of the supergene profile beneath the Guadalquivir basin sediments which involved a progressive change in the system conditions (i.e., Eh, pH, T). The deposition of the Guadalquivir basin sediments took place in the Miocene-Pliocene (Abad, 2007; Yesares et al., 2015), resulting in the burial of the deposit by a thick sequence of carbonate-rich sediments. The mineralogical assemblage formed during this stage (carbonates and sulfides), indicates that the Eh-pH conditions of the Las Cruces supergene environment were progressively more reducing due to the rise of the redox front, as well as more alkaline as a result of the buffering of carbonate-rich basinal fluids which circulated through the sedimentary supergene interface along late subvertical fractures that linked the sedimentary cover, the gossan, and the cementation zone (Fig. 8). At this stage, the intensity of supergene-related processes decreased as well as the influx of halide into the system due to the burial of the deposit and the later marine regression during the uppermost Miocene (Haq et al., 1987; Sierro et al., 1996). Hence, the Au mobilization via halide complexes decreased due to lesser availability and higher pH, resulting in the destabilization of such halide complexes (Krupp and Weiser, 1992; Usher et al., 2009).

During this period, basinal fluids enriched in precious metals migrated through the most permeable zones of the profile under neutral-to-alkaline and slightly oxidizing-to-reducing conditions. As a general rule, Au^{3+} halide complexes can only be transported short distances downward through the weathering profile due to low stability in less acidic environments (Mann, 1984; Saunders, 1993); hence, these complexes are not stable in the new system conditions. At neutral pH, however, Au^{3+}-halide ligands can be hydrolyzed to Au^{3+}-hydroxide-halide complexes, increasing their solubility (Krupp and Weiser, 1992; Usher et al., 2009; Ta et al., 2014). Alternatively, they could be reduced to Au^{1+}-halide complexes that are also more stable at neutral pH (Krupp and Weiser, 1992; Usher et al., 2009). In addition, in areas within the supergene profile under alkaline conditions, Au could be mobilized as Au^{3+}-hydroxide complexes, which are the most soluble ligands under these conditions (Krupp and Weiser, 1992; Usher et al., 2009; Ta et al., 2014). These mechanisms are sufficient for the transport and precipitation of Au throughout the weathering profile. Nevertheless, some proportion of the observed Au concentrations could have been fixed via micro-organism detoxification before reaching the gossan base or cementation zone. These Au^{3+} complexes would be highly toxic to some micro-organisms, which reduce the Au^{3+} complexes, thus resulting in precipitation of Au^0 nanoparticles (Reith et al., 2006, 2009; Brugger et al., 2013). These nanoparticles have not been identified to date within the Las Cruces supergene profile but have been reported in other gossans of the Iberian Pyrite Belt (Capitán, 2003; Viñals et al., 2003).

At this stage, alternative Au mobilization mechanisms via Au^{1+}-thiosulfate and Au^{1+}-bisulfide complexes, depending on the oxygen fugacity, are possible. Au^{1+}-thiosulfates are highly stable in neutral and slightly reducing conditions, as well as in the presence of carbonates (Webster and Mann, 1984; Renders and Seward, 1989; Benedetti and Bouleguè, 1991; Gray et al., 1992; Freyssinet et al., 2005; Tagirov et al., 2006). The pH-Eh condition suggested by the precipitation of siderite and calcite at this stage in the Las Cruces gossan enhances the stability of precious metal thiosulfate complexes (Yesares et al., 2014, 2015). These ligands could remain in solution over relatively long distances due to their slow kinetic transformation (Rolla and Chakrabarti, 1982). In addition, thiosulfate complexes could carry higher Au concentrations through the supergene profile, unaffected by possible Au-detoxifying microorganisms due to lesser toxicity of Au^{1+}-complexes (Brugger et al., 2013). Nevertheless, thiosulfate complexes formation involves mainly (bio)sulfur oxidation and weak (bio)sulfate reduction (Benedetti and Boulegue, 1991; Gray et al., 1992; Southam and Saunders, 2005; Lenke and Southam, 2006a; 2007; Southam et al., 2009; Shuster and Southam, 2015). In contrast, the Las Cruces gossan precipitated significant amounts of sulfides at this stage (Yesares et al., 2014, 2015). This mineral paragenesis (siderite ± galena within the gossan, and cinnabar + Ag-sulfosalts within fault breccias in the cementation zone) involves a reducing solution and (bio)sulfur reduction, which constrains the role of thiosulfate complexes as the only mobilization mechanism throughout the supergene profile. In zones where solutions were more reducing, thiosulfate complexes could have been reduced to bisulfide complexes due to their high solubility under low oxygen fugacity and near neutral conditions, as well as in equilibrium with pyrite (Stroffegen, 1986; Webster, 1986; Huston and Large, 1989; Renders and Seward, 1989; Vlassopoulos and Wood 1990; Benedetti and Boulegue, 1991; Gray et al., 1992; Tagirov et al., 2006). Furthermore, late-vertical fault systems acted as high permeability conduits driving the Au-Ag–enriched basinal fluids, with precious metals thiosulfate and/or bisulfide complexes as stable compounds in solution, until reaching the cementation zone (Fig. 9).

Regarding Au precipitation during the early gossan formation, high-fineness Au associated with the Fe-oxide facies at the upper gossan was formed as a result of the separation of

Au and Ag chlorides on ferrolysis (Mann, 1984; Saunders, 1993; Karasyova et al., 1998; Ran et al., 2002; Cohen and Waite, 2004). During ferrolysis-related processes, Au precipitated by reduction of Au-chloride complexes. However, Ag-chloride complexes are not precipitated as native Ag by oxidation of Fe^{2+} because the redox potential for Ag/AgCl is below that of the Fe^{2+}/Fe^{3+} couple (Mann, 1984; Saunders, 1993). Despite the limited solubility of Ag-halide minerals, Ag-chloride complexes can remain in solution, increasing their solubility in high chloride ion concentration groundwater and in the presence of Fe^{+2} (Mann, 1984; Saunders, 1993). Therefore, Ag-chloride complexes were separated and transported downward, enhancing the purity of gold grains (Saunders, 1993; Hough et al., 2009). In the Las Cruces case, the processes involved in Au precipitation give a wide range of morphologies including reniform, platy, and subrounded coarse particles (Fig. 5). Recently, the possibility of supergene Au enrichment linked to biogenic-related processes has been a topic of discussion (Reith et al., 2006; 2010; 2013; Southam et al., 2009; Fairbrother et al., 2012; Shuster and Southam, 2015). In this way, very fine (1–25-μm) reniform Au particles have been reported related to biological activity (Lengke et al., 2006a; Reith and McPhail, 2006; Reith et al., 2009, 2013; Southam et al., 2009). Moreover, other morphologies, including fine octahedral and hexagonal crystals (5–15 μm) have been attributed to similar biological genesis (Lengke et al., 2006b, c; Southam et al., 2009). In addition, it has been demonstrated that biomediated Au nanoparticles can aggregate rapidly by a biofilm to form coarse nuggets (4 to 5-mm). These coarse Au particles typically have surfaces composed of fine aggregates of biofilm-like Au (Reith et al., 2006, 2010; Shuster and Southam, 2015). In the Las Cruces gossan, several Au shapes have been described; however, most of these particles have grain sizes significantly larger than those reported as microbially mediated Au grains. Furthermore, at the time of writing, no evidence of nanoparticles accretion by biofilm has been observed on the surface of the Las Cruces Au grains (Fig. 5), as pointed out in other studies (Reith et al., 2006; Shuster and Southam, 2015) and as suggested for Las Cruces by Tornos et al. (2014). Thus, the different textures of Au particles reported from the Las Cruces supergene profile are not sufficient evidence by themselves to link their genesis to bacteriogenic processes. It should be noted that there could be a small proportion of Au nanoparticles dispersed throughout the gossan that are too small to have been detected in the present study, and these could have resulted from a Au biogenic precipitation mechanism.

Regarding Au precipitation mechanisms during the late evolution of the Las Cruces deposit, medium-fineness Au particles formed related to the gossan base and the fault breccias in the cementation zone. This later stage of the gossan evolution beneath the sedimentary cover led to gossan reduction and carbonatization (Fig. 9; Yesares et al., 2015), resulting in the precipitation of siderite, galena, and Fe-sulfides linked to the gossan profile (Yesares et al., 2015; Fig. 3A), as well as cinnabar, Ag-sulfides, and sulfosalts related to reduced lithologies such as black shales from the gossan base, and pyritic fault gouge from the cementation zone (Fig. 4A, B). Formation of cinnabar, Ag-sulfides, and sulfosalts from reduced percolating fluids associated with those reduced lithologies involved desulfurization in the Au-bearing solutions (Huston and Large, 1989; Williams et al., 2009). Therefore, these processes resulted in the destabilization of the aqueous Au^{1+}-sulfur carrier complexes and the formation of medium-fineness and subrounded Au grains (Figs. 4, 6, 7). Au precipitation at this stage involved the reduction of aqueous Au^{1+}-sulfur species to elemental Au likely at contact with the preexisting sulfides such as pyrite fault gouge in the cementation zone or even cinnabar and Ag-sulfosalts previously formed. As a consequence, Au fillings of interstices and Au coatings of sulfides can be observed. This Au precipitation mechanism by adsorption of Au complexes on sulfides has been described by Jean and Bancroft (1985), Hyland and Bancroft (1989), Renders and Seward (1989) and Schoonen et al. (1992). That Au and Ag sulfur complexes have similar solubilities and that both precipitated under similar pH and Eh conditions (Webster and Mann, 1984; Stoffrengen, 1986; Renders and Seward, 1989; Freyssinet., et al 2005), explains the presence of medium-fineness gold particles in the Las Cruces gossan (Figs. 4, 6, 7 and 9). In addition, these processes are believed to be responsible for the observed compositional variations of Au grains formed at this stage (Figs. 6, 7). Moreover, Au precipitation from sulfur complexes could be also favored by bacterial activity, resulting in Au crystals incorporated into the newly formed sulfide minerals (Lenke and Southam, 2006; 2007; Reith et al., 2007; 2013; Shuster and Southam, 2015). For instance, sulfate-reducing bacteria are able to reduce thiosulfate complexes to hydrogen sulfide (H_2S), leading to metal ion precipitation and subsequent formation of metal sulfides via bacterial detoxification. These processes destabilize the Au in solution, which can be incorporated into the newly formed sulfide as nanoparticles and or/ bioforms (Lengke and Southam, 2006a; 2007; Reith et al., 2007; Reith et al., 2013).

This later gold-bearing mineralization in the Las Cruces supergene profile differs from common Au-enriched gossans in the Iberian Pyrite Belt. Due to paleogeography, most deposits in the Iberian Pyrite Belt have not been covered by Tertiary basins (Strauss and Madel, 1974). Hence, only some profiles were involved in the weathering stage and precious metal concentration processes that are commonly described for Iberian Pyrite Belt deposits (Capitán et al., 2003; Capitan, 2006; Velasco et al., 2013) and deposits elsewhere (Grey et al., 1992; Freyssinet et al., 2005). In this way, Au in Iberian Pyrite Belt supergene mineralization has been reported exclusively as related to oxidized facies, including Fe-oxyhydroxides and sulfates (e.g., Riotinto: Viñals et al., 1995; Sanchez et al., 1996; Roca et al., 1999; Tharsis: Capitán et al., 2003; Capitán, 2006; Lomero-Poyatos: Velasco et al., 2013). Gold grains in these deposits are very fine grained, with subrounded morphologies (e.g., micrometer-sized subrounded, free-Au grains at Filón Sur Tharsis gossan, Capitán et al., 2003; submicroscopic- to 1-μm Au particles at Riotinto gossan, Viñals et al., 1995). Analogous textural features have been reported for other gossans elsewhere. As a general rule, Au in weathering profiles occurs as micrometer-sized grains up to 50 μm as free particles or associated with Fe-oxihydroxides and minor sulfates (Freyssinet et al., 2005). Examples of these supergene Au features have been reported at Zapdno-Ozeroe in South Urals (Belogub et al., 2003); at the TAG and for the Cyprus Troodos

Ophiolite (Herzig et al., 1991); at the Brasileiro Au deposit, Bahia, Brazil (Vasconcelos and Kyle, 1991); and at Cerro de Maimón, Dominican Republic (Andreu et al., 2014).

Conclusions

The supergene Au mineralization in the Las Cruces deposit differs significantly from Au-rich gossans elsewhere, including those found in the Iberian Pyrite Belt, in the following ways: (1) The Las Cruces deposit has a higher grade of Au than that found in other Iberian Pyrite Belt supergene profiles; (2) the Las Cruces Au distribution through the supergene profile and the Au-bearing lithologies are more variable than other Iberian Pyrite Belt deposits, including Fe-oxide facies dispersed in the upper part of the gossan, leached black shale levels at the gossan base, and fault breccia-related Au-Ag–rich secondary ore in the cementation zone (these last two Au-rich lithologies have not been described before in the Iberian Pyrite Belt); (3) Au particle sizes, fineness, textural features, and mineral associations are also different in Las Cruces in comparison with other Iberian Pyrite Belt supergene profiles. At Las Cruces, Au particles in Fe-oxide facies occur as coarse Au grains of high fineness associated with nadorite. Au linked to leached black shale levels occurs as coarse Au-Ag-Hg amalgams, whereas Au related to subvertical fault gouge in the cementation zone appears as relatively fine-grained particles of medium fineness associated with cinnabar, pyrargyrite, and proustite.

As in other Iberian Pyrite Belt deposits, the supergene Au concentration at the Las Cruces deposit is the result of Au leaching of the primary sulfides during weathering, whereas the further evolution of the Las Cruces deposit beneath the sediments of the Guadalquivir basin makes the Las Cruces Au mineralization unique.

The existence of three different Au ore types in the Las Cruces supergene profile suggests that more than one mechanism was involved in Au dissolution, mobilization, and precipitation. The occurrence of high-fineness Au associated with Pb-halides in the Fe-oxides facies involves Au chemical refining produced by precious metal mobilization during the oxidation of primary ores via halide complexes. These events took place during the deposit exhumation in Miocene times. Gold grains precipitated in association with early gossan Fe-oxihydroxides, which were later replaced by carbonates and sulfides.

After the deposition of the overlying sediments, the supergene profile redox conditions were progressively more reducing due to the rise of the redox front, and more alkaline as a result of the buffering of basinal fluids that circulated pervasively through the sediment-supergene profile interface along late subvertical fractures that linked the sedimentary cover, gossan, and cementation zone. The progressive change in the physico-chemical conditions of the Au-bearing solution resulted in precious metal migration through the profile linked to several ligands such as hydroxidehalide, hydroxide, and thiosulfate and bisulfide complexes. Au carrier ligands reached the gossan base and the cementation zone, resulting in the destabilization of the complexes and formation of Au-Ag-Hg amalgams and medium-fineness Au, both related to reduced lithologies such as black shales from the gossan base and pyritic fault gouge from the cementation zone.

The Au mobilization and precipitation mechanisms proposed for the Las Cruces supergene profile, with complexly changing redox conditions, could help to explain other supergene Au deposits that are less well understood. Moreover, the Las Cruces deposit irregularities and the precious metal mobilization-precipitation processes associated with the supergene profile evolution after the sedimentary cover deposition resulted in higher Au grades at Las Cruces than other Iberian Pyrite Belt deposits. Therefore, Iberian Pyrite Belt areas covered by Tertiary basins are a new target for precious metal exploration associated with supergene profiles developed from massive sulfides.

Acknowledgments

This research is a contribution to projects P-S Anoxia (CGL2011-30011) and Metodica (CGL2010-21956-C02-02), which are supported by the Spanish government. The authors thank Cobre Las Cruces S.A. for the field assistance and the ongoing collaboration. We are also grateful to Joël Brugger, Steve Hill, and Tim Baker for their constructive suggestions to improve the manuscript.

REFERENCES

Abad, M., 2007, La transgresión Tortoniense en el margen pasivo de la Cuenca del Guadalquivir: Unpublished Ph.D. thesis, Spain University of Huelva, 510 p.

Aiglsperger, T., Proenza, J.A., Zaccarini, F., Lewis, J.F., Garuti, G., Labrador, M., and Longo, F., 2014, Platinum group minerals (PGM) in the Falcondo Ni-laterite deposit, Loma Caribe peridotite (Dominican Republic): Mineralium Deposita, v. 50, p. 105–123.

Andreu, E., Torró, L., Proenza, J.A., Domenecha, C., García-Casco, A., Villanova de Benavent, C., Chavez, C., Espaillat, J., and Lewis, J.F., 2015, Weathering profile of the Cerro de Maimón VMS deposit (Dominican Republic): Textures, mineralogy, gossan evolution and mobility of Au and Ag: Ore Geology Reviews, v. 65, p. 165–179.

Almodóvar, G.R., Sáez, R., Pons, J.M., Maestre, A., Toscano, M., and Pascual, E., 1998, Geology and genesis of the Aznalcóllar massive sulphide deposits, Iberian Pyrite Belt, Spain: Mineralium Deposita, v. 33, p. 111–136.

Arribas, A., 1998, Los yacimientos de oro asociados con las monteras limoníticas de la FPI: Boletín Geológico y Minero, v. 109, p. 429–434.

Belogub, E., Novoselov, C., Spiro, B., and Yakovleva, B., 2003, Mineralogical and sulphur isotopic features of the supergene profile of Zapadno-Ozernoye massive sulphide and Au-bearing gossan deposit, South Urals: Mineralogical Magazine, v. 67, p. 339–354.

Benedetti, M., and Bouleguè, J., 1991, Mechanism of Au transfer and deposition in a supergene environment: Geochimica et Cosmochimica Acta, v. 55, p. 1539–1547.

Blake, C., 2008, The mineralogical characterisation and interpretation of a precious metal bearing fossil gossan, Las Cruces, Spain: Unpublished PhD thesis. Cardiff, University of Wales, 330 p.

Boyle, R.W., 1979, The geochemistry of Au and its deposits: Bulletin of the Geological Survey of Canada, v. 280, p. 1–584.

Boyle, D.R., 1997, Iodargyrite as an indicator of arid climatic conditions and its association with Au-bearing glacial tills of the Chibougamau-Chapais area, Quebec: Canadian Mineralogist, v. 35, p. 23–34.

Boyle, R.W., Alexander, W.M., Ashin, G.E.M., 1975, Some observations on the solubility of Au: Bulletin of the Geological Survey of Canada, p. 75–24.

Bowell, R.J., Foster, R.P., and Gize, A.P., 1993, The mobility of Au in tropical rain forest soils: Economic Geology, v. 88, p. 999–1016.

Brugger, J., Etschmann, B., Grosse, C., Plumridge, C., Kaminski, J., Paterson. D., Shar, S.S., Ta, C., Howard, D.I., Jonge, M.D., Ball, A.S., and Reith, F., 2013, Can biological toxicity drive the contrasting behavior of platinum and gold in surface environments?: Chemical Geology, v. 343, p. 99–110.

Butt, C.R.M., 1998, Supergene Au deposit: Journal of Australian Geology and Geophysics, v. 17, p. 89–96.

Capitán, M.A., 2006, Mineralogía y geoquímica de la alteración superficial de depósitos de sulfuros masivos en la Faja Pirítica Ibérica: Unpublished Ph.D. thesis, Spain, University of Huelva, 260 p.

Capitán, M.A., Nieto, J.M., Sáez, R., Almodóvar, G.R., 2003, Caracterización textural y mineralógica del gossan de Filón Sur (Tharsis, Huelva): Boletíin. Sociedad Española de Mineralógia, v. 26, p. 45–58.

Carvalho, D., 1976, Consideraçoes sobre o vulcanismo da regiao de Cercal-Odemira. Suas relaçoes com a Faixa Piritosa: Comunicaçao do Serviço Geologicodo Portal, v. 60, p. 215–238.

Cohen, D.R., Waite, T.D., 2004, Interaction of aqueous Au species with goethite, smectite and kaolinite: Geochemistry-Exploration Environment Analysis, v. 4, p. 279–287.

Doyle, M., Morrissey, C., and Sharp, G., 2003, The Las Cruces Orebody, Seville province, Andalucia, Spain, *in* Kelly, C.G., et al., eds., The Geology and genesis of Europe's major base metal deposits: Irish Association for Economic Geology, Dublin., p. 381–390.

Erlebacher, J., Aziz, M.J., Karma, A., Dimitrov, N., and Sieradzki, K., 2001, Evolution of nanoporosity in dealloying: Nature, v. 410, p. 450–453.

Essalhi, M., Sizaret, S., Barbanson, L., Chen, Y., Lagroix, F., Demory, F., Nieto, J.M., Sáez, R., and Capitán, M.A., 2011, A case study of the internal structures of gossans and weathering processes in the Iberian Pyrite Belt using magnetic fabrics and paleomagnetic dating: Mineralium Deposita, v. 46, p. 981–999.

Fairbrother, L., Brugger, J., Shapter, J., Laird, J.S., Southam, G., and Reith, F., 2012, Supergene Au transformation: Biogenic secondary and nanoparticulate Au from arid Australia: Chemical Geology, v. 320, p. 17–31.

Freyssinet, P., Butt, C.R.M., Morris, R.C., Piantone, P., 2005, Ore-forming processes related to lateritic weathering: Economic Geology 100th Anniversary Volume, p. 681–722.

Freyssinet, P.H., Zeegers, H., and Tardy, Y., 1989, Morphology and geochemistry of Au grains in lateritic profiles of southern Mali: Journal of Geochemical Exploration, v. 32, p. 17–31.

García de Miguel, J.M., 1990, Mineralogía, paragénesis y sucesión de los sulfuros masivos en la Faja Pirítica en el suroeste de la Península Ibérica: Boletín Geológico y Minero, v.101, p. 73–105.

García Palomero, F., Bedia Fernández, J.L., García Magariño, M., and Sides, E.J., 1986, Nuevas investigaciones y trabajos de evaluación de reservas de gossan en Minas de Riotinto: Boletín Geológico y Minero, v. 97, p. 622–642.

Golebiowska, B., Pieczka, A., Rzepa, G., Matyszkiewicz, J., Krajewski, M., 2010, Iodargyrite from Zalas (Cracow area, Poland) as an indicator of Oligocene-Miocene aridity in Central Europe: Palaeogeogr. Palaeoclimatol, v. 296, p. 130–137.

Gray, D.J., 2001, Hydrogeochemistry in the Yilgarn Craton: Geochemistry: Exploration, Environment, Analysis, v. 1, p. 253–264.

Gray, D.J., Butt, C.R.M., and Lawrance, L.M., 1992, The geochemistry of Au in lateritic terrains, *in* Butt, C.R.M., Zeegers, H., eds., regolith exploration geochemistry in tropical and subtropical terrains, Handbook of Exploration Geochemistry, v. 4, p. 461–482.

Groen, J.C., Craig, J.R., and Rimstidt, J.D., 1990, Au-rich rim formation on electrum grains in placers: Canadian Mineralogist, v. 28, p. 207–228.

Haq, B.U., Hardenbol, H., and Vail, P.R., 1987, Chronology of fluctuating sea levels since the Triassic: Science, v. 235, p. 1156–1167.

Herzig, P.M., Hannington, M.D., Scott, S.D., Maliotis, G., Rona, P.A., and Thompson, G., 1991, Au-rich sea-floor gossan in the Troodos Ophiolite and on the Mid-Atlantic Ridge: Economic Geology, v. 86, p. 1747–1755.

Hough, R.M., Butt, C.R.M., Reddy, S.M., and Verrall, M., 2007, Gold nuggets: supergene or hypogene?: Australian Journal of Earth Sciences, v. 54, p. 959–964.

Hough, R., Noble, R., Hitchen, G., Hart, G., Reddy, S., Saunders, M., Clode, P., Vaughan, D., Lowe, J., Gray, D., Butt, C.R., and Verrall, M., 2008, Naturally occurring Au nanoparticles and nanoplates: Geology, v. 36, p. 571–574.

Hough, R.M., Butt, C.R.M., and Fischer-Bühner, J., 2009, The crystallography, metallography and composition of Au: Elements, v. 5, p. 297–302.

Hough, R.M., Noble, R.R.P., and Reith, M., 2011, Natural Au nanoparticles: Ore Geology Reviews, v. 42, p. 55–61.

Huston, D.L., and Large, R.R., 1989. A chemical model for the concentration of gold in volcanogenic massive sulphide deposit: Ore Geology Reviews, v. 4, p. 171–200.

Hyland, M.M., and Bancroft, G.M., 1989, An XPS study of gold deposition at low temperatures on sulphide minerals: reducing agents: Geochimica et Cosmochimica Acta, v. 53, p. 367–372.

Jean, G.E., and Bancroft, G.M., 1985, An XPS and SEM study of gold deposition at low temperatures on sulphide minerals: concentration by adsorption/reduction: Geochimica et Cosmochimica Acta, v. 49, p. 979–987.

Karasyova, O.N., Ivanova, L.I., Lakshtanov, L.Z., Lovgren, L., and Sjoberg, S., 1998, Complexation of gold(III)-chloride at the surface of hematite: Aquatic Geochemistry, v. 4, p. 215–231.

Knight, F., 2000, The mineralogy, geochemistry and genesis of the secondary sulphide mineralization of the Las Cruces deposit, Spain: Unpublished PhD Thesis. Cardiff, University of Wales.

Krupp, R.E., and Weiser, T., 1992, On the stability of Au-Ag alloys in the weathering environment: Mineralium Deposita, v. 27, p. 268–275.

Lengke, M.F., and Southam, G., 2007, The deposition of elemental gold from gold(I)-thiosulfate complex mediated by sulfate-reducing bacterial conditions: Economic Geology, v. 102, p. 109–126.

Lengke, M., and Southam, G., 2006a, Bioaccumulation of Au by sulfate-reducing bacteria cultured in the presence of Au (I)-thiosulfate complex: Geochimica et Cosmochimica Acta, v. 70, p. 3646–3661.

Lengke, M., Fleet, M., and Southam, G., 2006b, Bioaccumulation of gold by filamentous cyanobacteria between 25 and 200°C: Geomicrobiology Journal, v. 23, p. 591–597.

Lengke, M., Ravel, B., Fleet, M., Wanger, G., Gordon, R., Southam, G., 2006c, Mechanisms of gold bioaccumulation by filamentous cyanobacteria from gold(III)-Chloride Complex: Environmental Science & Technology, v. 40, p. 6304–6309.

Leistel, J.M., Marcoux, E., Thiéblemont, D., Quesada, C., Sánchez, A., Almodóvar, G.R., Pascual, E., Sáez, R., 1998, The volcanic-hosted massive sulfide deposits of the Iberian Pyrite Belt. Review and preface to the thematic issue: Mineralium Deposita, v. 33, p. 2–30.

Mann, A.W., 1984, Mobility of Au and Ag in lateritic weathering profiles: some observations from Western Australia: Economic Geology, v. 79, p. 38–50.

Marcoux, E., Moelo, Y., Leistel, J.M., 1996, Compared ore mineralogy and geochemistry of the massive sulfide and stringer ore deposits of the Southern Spain: Mineralium Deposita, v. 31, p. 1–26.

Martín-Algarra, A., and Vera, J.A., 2004, La Cordillera Bética y las Baleares en el contexto de Mediterráneo Occidental, *in* Vera, J.A., eds., Geología de España, p. 352–354.

Moreno, C., Capitán, M.A., Doyle, M., Nieto, J.M., Ruiz, F., and Sáez, R., 2002, Edad mínima del gossan de Las Cruces: Implicaciones sobre el inicio de los ecosistemas extremos en la Faja Pirítica Ibérica: Geogaceta, v. 33, p. 67–70.

Nocete, F., Sáez, R., Bayona, M.R., Nieto, J.M., Paramo, A., López, P., Gilbarguchi, J.I., Inácio, N., García, S., and Rodríguez, J., 2014, Au in the southwest of the Iberian Peninsula during the 3rd Millennium BC: Journal of Archaeological Science, v. 41, p. 691–704.

Oliveira, D.P.S., Matos, J.X.M., Rosa, C.J.P., Rosa, D.R.N., Figueiredo, M.O., Silva, T.P., Guimarães, F., Carvalho, J.R.S., Pinto, Á.M.M., Relvas, J.R.M.S., and Reiser, F.K.M., 2011, The Lagoa Salgada orebody, Iberian Pyrite Belt, Portugal: Economic Geology, v. 106, p. 1111–1128.

Pérez-Asensio, J.N., Aguirre, J., Schmield, G., Civis, J., 2014, Messinian productivity changes in the northeastern Atlantic and their relationship to the closure of the Atlantic-Mediterranean gateway: Implications for Neogene palaeoclimate and palaeoceanography: Journal of the Geological Society, v. 171, p. 389–400.

Pinto, A.M.M., Relvas, F.J.M.R.S., Barriga, J.A.S., Munha, J., Pacheco, N., and Scott, S.D., 2005, Au mineralization in recent and ancient volcanic-hosted massive sulfides. The PACMANUS field and the Neves Corvo deposit: Mineral Deposit Research: Meeting the Global Challenge, v. 1 and 2, p. 683–686.

Ran, Y., Fu, J., Rate, A.W., and Gilkes, R.J., 2002, Adsorption of Au(I, III) complexes on Fe, Mn oxides and humic acid: Chemical Geology, v. 185, p. 33–49.

Reich, M., Palacios, C., Alvear, M., Cameron, E.M., Leybourne, M.I., and Deditius, A., 2009, Iodine-rich waters involved in supergene enrichment of the Mantos de la Luna argentiferous copper deposit, Atacama desert, Chile: Mineralium Deposita, v. 44, p. 719–722.

Reith, F., and Mcphail, D.C., 2006, Effect of resident microbiota on the solubilization of Au in soil from the Tomakin Park Au mine, New South Wales, Australia: Geochimica et Cosmochimica Acta, v. 70, p. 1421–1438.

Reith, F., Brugger, J., Zammit, C.M., Nies, D.H., and Southam, G., 2013, Geobiological cycling of gold: From fundamental process understanding to exploration solutons: Minerals, v. 3, p. 367–394.

Reith, F., Fairbrother, L., Nolze, G., Wilhelmi, O., Clode, P.L., Gregg, A., Parsons, J.E., Wakelin, S.A., Pring, A., Hough, R., Southam, G., and Brugger, J., 2010, Nanoparticle factories: Biofilms hold the key to Au dispersion and nugget formation: Geology, v. 38, p. 843–846.

Reith F., Lengke M.F., Falconer D., Craw, D., and Southam, G., 2007, The geomicrobiology of Au: International Society for Microbial Ecology, ISME Journal, v, 1, p. 567–584.

Reith, F., Rogers, S.L., McPhail, D.C., and Webb, D., 2006, Biomineralization of gold: Biofilms on bacterioform gold: Science, v. 313, p. 233–236.

Reith, F., Stewart, L., and Wakelin, S.A., 2012, Supergene Au transformation: Secondary and nano-particulate Au from southern New Zealand: Chemical Geology, v. 320, p. 32–45.

Renders, P.J.N., Seward, T.M., 1989, The stability of hydrosulphido and sulphido-complexes of Ag (I) and Au (I) at 25 C: Geochimica et Cosmochimica Acta, v. 53, p. 245–253.

Roca, A., Viñals, J., and Arranz, M. y Calero, J., 1999, Characterization and alkaline decomposition/cyanidation of beudantite-jarosite materials from Rio Tinto Gossan Ores: Canadian Metallurgical Quarterly, v. 38, p. 93–103.

Rolla, E., Chakrabarti, C.L., 1982, Kinetics of decomposition of tetrathionate, trithionate and thiosulphate in alkaline media: Environmental Science & Technology, v. 16, p. 852–857.

Rudashevsky, N.S., and Rudashevsky, V.N., 2006, Patent of Russian Federation #2281808, invention "Hydraulic Classifier," Moscow, 20 August 2006.

——2007, Patent of Russian Federation #69418, industrial (useful) model, "Device for separation of solid particles," Moscow, December 27, 2007.

Rudashevsky, N.S., Lupal, S.D., and Rudashevsky, V.N., 2001, The hydraulic classifier. Russian patent N2165300. Patent Cooperation Treaty PCT/Ru 01/00123.

Sáez, R., Pascual, E., Toscano, M., Almodóvar, G.R., 1999, The Iberian type of volcanosedimentary massive sulfide deposits: Mineralium Deposita, v. 34, p. 549–570.

Sanchez, L., Cruells, M., Roca, A., 1996, Sulhidization-cyanidation of jarosite species: Applicability to the gossan ores of Rio Tinto: Hydrometallurgy, v. 42, p. 35–49.

Saunders, J.A., 1993, Supergene oxidation of bonanza Au-Ag veins at the Sleeper deposit, Nevada, USA: Implications for hydrochemical exploration in the Great Basin: Journal of Geochemical Exploration, v. 47, p. 359–375.

Schermerhorn, L.J.G., 1971, An outline stratigraphy of the Iberian Pyrite Belt: Boletín Geologico y Minero, v. 82, p. 239–268.

Schoonen, M.A., Fisher, N.S., and Wente, M., 1992, Gold sorption onto pyrite and goethite: A radiotracer study: Geochimica et Cosmochimica Acta, v. 56, p. 1801–1814.

Shuster, J., and Southam, G., 2015, The in-vitro "growth" of gold grains: Geology, v. 43, p. 79–82.

Sierro, F.J., Gonzalez-Delgado, J.A., Dabrio, C., Flores, J.A., and Civis, J., 1996, Late Neogene depositional sequences in the foreland basin of Guadalquivir (SW Spain), *in* Friends, P.F., and Dabrio, C., eds., Tertiary basins of Spain: Cambridge University Press, p. 339–345.

Silva, J.B., Oliveira, J.T., and Ribeiro, A., 1990, South Portuguese zone: Structural outline, *in* Dallmeyer, R.D., and Martinez Garcia, E., eds., Pre-Mesozoic geology of Iberia: Berlin, Springer-Verlag, p. 348–362.

Simancas, J.F., 1983, Geología de la extremidad oriental de la zona surportuguesa: Unpublished PhD thesis, Spain, University of Granada, 439 p.

Southam, G., Lengke, M.F., Fairbrother, L., and Reith, F., 2009, The biogeochemistry of Au: Elements, v. 5, p. 303–307.

Southam, G., and Saunders, J.A., 2005, The geomicrobiology of ore deposits: Economic Geology, v. 100, p. 1067–1084.

Stroffregen, R., 1986, Observations on the behaviour of Au during supergene oxidation at Summitville, Colorado, USA and implications for electrum stability in the weathering environment: Applied Geochemistry, v. 2, p. 549–558.

Ta, C., Reith, F., Brugger, J., Pring, A., and Lenehan, C., 2014, Analysis of gold(I/III)-complexes by HPLC-ICP-MS demonstrates gold(III) stability in surface waters: Environmental Science & Technology, v. 48, p. 5737–5744.

Tagirov. B.R., Baranova, N.N., Zotov, A.V., Schott, J., and Bannykn, L.N., 2006, Experimental determination of the stabilities of $Au_2S_{(cr)}$ at 25ºC and $Au(HS)_2^-$ at 25–250ºC: Geochimica et Cosmochimica Acta, v. 70, p. 3689–3701.

Tornos, F., Velasco, F., Menor-Salván, C., Delgado, A., Slack, J., and Escobar, J.M., 2014, Formation of recent Pb-Ag-Au mineralization by potential subsurface microbial activity: Nature Communications, v. 5, p. 1–8.

Usher, A., McPhail, D.C., Brugger, J.A, 2009, Spectrophotometric study of aqueous Au(III) halide–hydroxide complexes at 25–80°C: Geochimica et Cosmochimica Acta, v. 73, p. 3359–3380.

Vasconcelos, P., and Kyle, J.R., 1991. Supergene geochemistry and crystal morphology of Au in a semiarid weathering environment: application to Au exploration: Journal of Geochemical Exploration, v. 40, p. 115–132.

Velasco, F., Herrero, J.M., Suárez, S., Yusta, I., Alvaro, A., and Tornos, T., 2013, Supergene features and evolution of gossans capping massive sulphide deposits in the Iberian Pyrite Belt: Ore Geology Reviews, v. 53, p. 181–203.

Velasco, F., Yanguas, A., Sánchez-España, J., Yusta, I., Herrero, J.M., Santos, A., and Prada, J.M., 1999, in Stanley, C.J., Eds., A Hg-rich Au mineral association in the Migollas massive sulfide deposit from the IPB, Spain: Balkema, v. 2, p. 609–612.

Viñals, J., Roca, A., Cruells, M., and Nuñez, C., 1995, Characterisation and cyanidation of Rio Tinto Gossan ores: Canadian Metallurgical Quarterly, v. 34, p. 115–122.

Vlassopoulos, D., and Wood, S.A., 1990, Gold speciation in natural waters: I. Solubility and hydrolysis reactions of gold in a aqueous solution: Geochimica et Cosmochimica Acta, v. 54, p. 3–12.

Webster, J.G., 1986, The solubility of Au and Ag in the system Au-Ag-S-O_2-H_2O at 25°C and 1 atm: Geochimica et Cosmochimica Acta, v. 50, p. 245–255.

Webster, J.G., and Mann, A.W., 1984, The influence of climate, geomorphology and primary geology on the supergene migration of Au and Ag: Journal of Geochemical Exploration, v. 22, p. 21–42.

Williams, D., 1950, Gossanized breccia-ores, jarosites and jaspers at Rio Tinto Spain: Transactions of the Institution of Mining and Metallurgy, v. 526, p. 1–12.

Williams-Jones, A.E., Bowell, R.J., Migdisov, A.A., 2009, Au in solution: Elements, v. 5, p. 281–287.

Yesares, L., Sáez, R., Nieto, J.M., Almodóvar, G.R, and Cooper, S., 2014, Supergene enrichment of precious metals by natural amalgamation in the Las Cruces weathering profile (Iberian Pyrite Belt, SW Spain): Ore Geology Reviews, v. 58, p. 14–26.

Yesares, L., Sáez, R., Nieto, J.M., Almodóvar, G.R., Gómez, C., and Escobar, J.M., 2015, The Las Cruces deposit, Iberian Pyrite Belt, Spain: Ore Geology Reviews, v. 66: 25–46.

Appendix Table 1. EPMA Analysis (wt %) of Gold Ore Types in the Las Cruces Supergene Profile

Gold type	Samples	Au	Ag	Cu	Sb	Fe	Se	Pb	S	Hg	Total	Fineness
Gold grains from Fe-oxide facies of the upper gossan												
	1-1	98.73	n.d	n.d	n.d	n.d	n.d	n.d	0.05	0.06	98.85	1,000.00
	1-3	99.89	n.d	n.d	0.10	n.d	n.d	n.d	0.05	n.d	100.056	1,000.00
	1-4	99.53	0.29	n.d	n.d	n.d	n.d	0.15	0.06	n.d	99.78	997.09
	1-5	99.34	n.d	n.d	n.d	n.d	0.03	n.d	0.04	n.d	99.43	1,000.00
	1-6	92.55	0.67	0.07	0.08	n.d	0.07	n.d	0.15	n.d	93.61	992.80
	1-7	96.81	0.40	n.d	0.14	n.d	n.d	n.d	0.05	n.d	97.04	995.88
	1-8	99.43	n.d	n.d	0.12	n.d	0.02	n.d	0.03	n.d	99.62	1,000.00
	1-9	100.26	n.d	n.d	n.d	0.10	n.d	n.d	0.04	n.d	100.41	1,000.00
	1-10	99.09	n.d	n.d	n.d	0.02	n.d	n.d	0.04	n.d	99.15	1,000.00
	1-11	100.00	0.31	0.03	n.d	n.d	n.d	n.d	0.07	0.08	100.22	996.91
	1-12	100.39	0.40	n.d	n.d	n.d	n.d	n.d	0.04	n.d	100.47	996.03
	1-13	99.71	n.d	n.d	n.d	n.d	n.d	n.d	0.06	n.d	99.77	1,000.00
	1-14	97.94	0.34	0.03	n.d	n.d	n.d	n.d	0.08	n.d	98.41	996.50
	1-15	98.94	0.38	0.02	n.d	n.d	n.d	n.d	0.07	n.d	99.42	996.17
	1-16	100.47	n.d	n.d	n.d	n.d	n.d	n.d	0.04	n.d	100.51	1,000.00
	1-17	99.69	0.30	n.d	n.d	0.01	n.d	n.d	0.02	n.d	99.76	997.00
	1-18	100.36	n.d	n.d	n.d	n.d	n.d	n.d	0.04	n.d	100.41	1,000.00
	1-19	99.60	n.d	n.d	n.d	n.d	n.d	n.d	0.04	n.d	99.645	1,000.00
	1-20	96.56	n.d	n.d	0.21	n.d	n.d	n.d	0.05	n.d	96.83	1,000.00
	1-21	98.12	n.d	n.d	0.18	n.d	n.d	n.d	0.05	n.d	98.36	1,000.00
	1-22	99.24	0.24	n.d	0.08	0.01	n.d	0.07	0.06	n.d	99.72	997.56
	1-23	99.74	n.d	n.d	n.d	n.d	0.02	n.d	0.03	n.d	99.80	1,000.00
	1-24	99.40	n.d	n.d	n.d	n.d	n.d	n.d	0.05	n.d	99.46	1,000.00
	1-25	98.90	n.d	n.d	n.d	n.d	n.d	0.16	0.07	0.00	99.15	1,000.00
	1-26	98.79	n.d	n.d	n.d	n.d	0.03	n.d	0.05	n.d	98.87	1,000.00
	1-27	98.49	n.d	n.d	n.d	n.d	n.d	n.d	0.03	n.d	98.53	1,000.00
	1-28	98.45	n.d	n.d	n.d	n.d	n.d	0.12	0.09	n.d	98.67	1,000.00
	1-29	98.20	n.d	n.d	n.d	0.02	0.02	n.d	0.04	n.d	98.29	1,000.00
	1-30	98.72	n.d	n.d	0.09	0.02	n.d	0.05	0.06	n.d	98.96	1,000.00
	1-31	98.76	n.d	n.d	0.11	n.d	n.d	n.d	0.05	n.d	98.93	1,000.00
	1-32	98.09	n.d	n.d	n.d	0.01	n.d	n.d	0.09	n.d	98.19	1,000.00
	1-33	99.59	n.d	n.d	n.d	n.d	n.d	n.d	0.03	n.d	99.62	1,000.00
	1-34	99.01	n.d	n.d	n.d	n.d	n.d	n.d	0.04	n.d	99.06	1,000.00
	1-35	98.58	n.d	n.d	n.d	n.d	0.02	n.d	0.05	n.d	98.66	1,000.00
	1-36	98.90	0.29	n.d	n.d	n.d	n.d	0.10	0.06	n.d	99.11	997.07
	1-37	98.32	n.d	n.d	n.d	n.d	n.d	n.d	0.06	n.d	98.38	1,000.00
	1-38	99.74	n.d	n.d	0.07	n.d	n.d	n.d	0.03	n.d	99.85	1,000.00
	1-40	98.78	n.d	n.d	0.09	n.d	0.02	n.d	0.05	n.d	98.96	1,000.00
	1-41	99.54	n.d	n.d	0.07	0.01	n.d	n.d	0.06	n.d	99.70	1,000.00
	1-42	99.01	n.d	n.d	0.09	n.d	n.d	n.d	0.05	n.d	99.16	1,000.00
	1-43	98.51	n.d	n.d	n.d	n.d	n.d	0.06	0.06	n.d	98.64	1,000.00
	1-44	99.63	0.30	n.d	n.d	0.01	n.d	n.d	0.03	0.02	99.73	996.69
	1-45	99.68	n.d	n.d	n.d	0.02	0.05	n.d	0.04	n.d	99.81	1,000.00
	1-46	98.40	n.d	n.d	n.d	n.d	n.d	n.d	0.06	n.d	98.46	1,000.00
	1-47	99.40	n.d	n.d	0.14	n.d	n.d	n.d	0.03	n.d	99.58	1,000.00
	1-48	99.45	n.d	n.d	n.d	0.01	0.05	n.d	0.06	n.d	99.58	1,000.00
	1-49	97.52	0.28	n.d	0.09	n.d	n.d	n.d	0.03	n.d	97.68	997.13
	1-50	99.33	n.d	n.d	0.09	0.03	n.d	n.d	0.08	n.d	99.54	1,000.00
	1-51	98.63	0.27	n.d	n.d	n.d	n.d	n.d	0.07	n.d	98.73	997.27
	1-52	99.61	0.16	0.04	n.d	n.d	n.d	n.d	0.04	n.d	99.86	998.36
	1-53	99.71	n.d	n.d	n.d	n.d	0.07	n.d	0.05	n.d	99.83	1,000.00
	1-54	99.82	n.d	0.02	n.d	n.d	0.02	n.d	0.02	n.d	99.89	1,000.00
	1-55	99.28	n.d	n.d	n.d	0.03	n.d	n.d	0.03	n.d	99.35	1,000.00
	1-56	99.21	n.d	n.d	n.d	n.d	n.d	0.05	0.02	n.d	99.29	1,000.00
	1-57	97.97	1.32	0.09	n.d	n.d	n.d	n.d	0.04	n.d	99.44	986.64
	1-58	98.56	n.d	n.d	n.d	n.d	0.03	n.d	0.03	n.d	98.63	1,000.00
	1-59	99.14	n.d	n.d	0.12	0.02	n.d	n.d	0.04	n.d	99.34	1,000.00
	1-60	99.91	n.d	n.d	n.d	n.d	0.03	n.d	0.05	n.d	100.00	1,000.00
	1-61	98.85	n.d	n.d	n.d	n.d	n.d	n.d	0.02	n.d	98.87	1,000.00
	1-62	99.17	n.d	n.d	n.d	n.d	0.02	n.d	0.05	0.10	99.36	1,000.00
	1-63	98.25	n.d	n.d	n.d	n.d	n.d	n.d	0.04	n.d	98.29	1,000.00
	1-64	98.68	n.d	n.d	0.11	n.d	n.d	n.d	0.02	n.d	98.82	1,000.00
	1-65	99.13	n.d	n.d	n.d	n.d	n.d	0.07	0.05	n.d	99.26	1,000.00
	1-66	98.34	n.d	n.d	n.d	0.01	0.04	n.d	0.04	n.d	98.45	1,000.00
	1-67	98.31	n.d	0.03	n.d	n.d	n.d	n.d	0.07	n.d	98.41	1,000.00
	1-68	99.12	n.d	n.d	n.d	n.d	0.03	n.d	0.07	n.d	99.23	1,000.00
	1-69	98.51	0.25	n.d	n.d	n.d	0.03	n.d	0.06	n.d	98.63	997.46

Appendix Table 1. EPMA Analysis (wt %) of Gold Ore Types in the Las Cruces Supergene Profile

Gold type	Samples	Au	Ag	Cu	Sb	Fe	Se	Pb	S	Hg	Total	Fineness
Gold grains from Fe-oxide facies of the upper gossan												
	1-71	98.15	n.d	0.05	n.d	n.d	n.d	0.05	0.04	n.d	98.31	1,000.00
	1-72	99.27	n.d	n.d	0.09	n.d	n.d	n.d	0.03	n.d	99.41	1,000.00
	1-73	98.50	n.d	n.d	n.d	0.02	n.d	0.05	0.05	n.d	98.64	1,000.00
	1-74	99.19	n.d	n.d	0.09	0.04	0.06	0.08	0.04	n.d	99.52	1,000.00
	1-75	96.35	n.d	n.d	n.d	0.02	n.d	n.d	0.06	n.d	96.44	1,000.00
	1-76	98.79	n.d	n.d	n.d	n.d	n.d	n.d	0.05	n.d	98.84	1,000.00
	1-77	98.92	n.d	n.d	n.d	n.d	0.04	n.d	0.05	n.d	99.02	1,000.00
	1-78	99.34	n.d	n.d	n.d	n.d	n.d	n.d	0.05	0.05	99.44	1,000.00
	1-79	99.59	n.d	n.d	0.17	n.d	n.d	n.d	0.06	n.d	99.83	1,000.00
	1-80	96.49	n.d	n.d	n.d	0.01	n.d	n.d	0.11	n.d	96.62	1,000.00
	1-81	99.25	n.d	n.d	n.d	n.d	n.d	n.d	0.04	n.d	99.30	1,000.00
	1-84	99.30	n.d	n.d	n.d	n.d	n.d	n.d	0.06	n.d	99.37	1,000.00
	1-85	99.38	n.d	n.d	n.d	n.d	n.d	n.d	0.06	n.d	99.44	1,000.00
	1-86	99.75	0.38	n.d	n.d	n.d	n.d	n.d	0.02	n.d	99.81	996.20
	1-87	99.90	n.d	n.d	n.d	n.d	n.d	n.d	0.05	n.d	99.95	1,000.00
	1-88	99.19	n.d	n.d	0.14	0.01	n.d	0.07	0.05	n.d	99.48	1,000.00
	1-89	98.12	n.d	0.05	n.d	n.d	n.d	0.10	0.09	n.d	98.37	1,000.00
	1-90	99.07	n.d	n.d	n.d	n.d	n.d	n.d	0.06	n.d	99.14	1,000.00
	1-91	98.46	n.d	0.03	n.d	0.01	0.02	n.d	0.04	n.d	98.58	1,000.00
	1-92	98.43	n.d	n.d	n.d	n.d	0.03	n.d	0.06	n.d	98.53	1,000.00
	1-93	98.38	n.d	n.d	n.d	n.d	0.03	n.d	0.05	n.d	98.48	1,000.00
	1-94	98.66	0.37	n.d	0.08	0.06	0.02	n.d	0.10	n.d	99.31	996.25
	1-95	99.38	0.24	n.d	n.d	0.03	0.02	n.d	0.06	n.d	99.74	997.58
	1-96	99.43	0.14	n.d	n.d	0.01	0.02	n.d	0.06	0.08	99.76	998.58
	1-97	100.25	n.d	n.d	n.d	n.d	0.05	n.d	0.05	n.d	100.35	1,000.00
	1-98	99.03	n.d	n.d	0.07	n.d	n.d	n.d	0.04	n.d	99.16	1,000.00
	1-99	99.60	0.37	n.d	n.d	0.02	0.02	n.d	0.08	n.d	100.10	996.24
	1-100	98.90	0.39	n.d	0.09	0.02	0.03	n.d	0.14	n.d	99.60	996.02
	1-101	97.27	n.d	n.d	n.d	n.d	0.02	n.d	0.06	n.d	97.36	1,000.00
	1-102	99.73	n.d	n.d	n.d	n.d	n.d	n.d	0.09	n.d	99.82	1,000.00
	1-103	99.77	0.24	n.d	n.d	n.d	0.02	n.d	0.04	n.d	99.87	997.60
	1-104	99.44	0.28	0.05	n.d	0.04	n.d	0.11	0.09	n.d	100.04	997.12
	1-105	100.10	n.d	0.05	n.d	n.d	0.04	n.d	0.04	n.d	100.24	1,000.00
	1-106	98.83	0.22	n.d	n.d	0.11	0.03	0.15	0.06	n.d	99.40	997.77
	1-107	97.99	0.58	n.d	n.d	n.d	n.d	0.05	0.06	n.d	98.68	994.09
	1-108	99.34	0.59	n.d	n.d	n.d	n.d	n.d	0.11	n.d	100.05	994.04
	1-109	98.43	0.62	n.d	0.07	n.d	0.05	n.d	0.11	n.d	99.30	993.69
	1-110	99.36	n.d	n.d	0.08	n.d	0.03	n.d	0.06	n.d	99.54	1,000.00
	1-111	100.12	n.d	n.d	n.d	n.d	n.d	n.d	0.04	n.d	100.17	1,000.00
	1-112	99.10	n.d	n.d	n.d	n.d	n.d	n.d	0.04	n.d	99.15	1,000.00
	1-114	98.89	n.d	n.d	n.d	n.d	n.d	0.04	0.06	0.30	99.30	1,000.00
	1-115	99.28	n.d	n.d	n.d	n.d	n.d	n.d	0.0	n.d	99.36	1,000.00
	1-116	100.12	n.d	n.d	0.08	n.d	n.d	n.d	0.07	n.d	100.29	1,000.00
	1-117	99.14	n.d	n.d	n.d	0.01	n.d	n.d	0.07	n.d	99.24	1,000.00
	1-118	99.86	n.d	0.09	0.08	0.02	n.d	n.d	0.05	n.d	100.12	1,000.00
	1-119	99.83	n.d	n.d	n.d	0.02	n.d	n.d	0.03	n.d	99.89	1,000.00
	1-120	100.21	n.d	n.d	n.d	n.d	n.d	n.d	0.07	n.d	100.29	1,000.00
	1-121	99.51	n.d	n.d	n.d	n.d	0.03	n.d	0.04	n.d	99.59	1,000.00
	1-122	99.33	n.d	n.d	0.15	0.07	n.d	n.d	0.04	n.d	99.60	1,000.00
	1-123	99.66	n.d	n.d	n.d	n.d	n.d	n.d	0.06	n.d	99.73	1,000.00
	1-124	100.19	n.d	n.d	n.d	0.01	n.d	n.d	0.04	n.d	100.25	1,000.00
	1-125	99.41	n.d	0.05	n.d	n.d	n.d	n.d	0.05	n.d	99.52	1,000.00
	1-126	100.55	n.d	n.d	0.07	n.d	0.04	n.d	0.03	0.04	100.74	1,000.00
	1-127	98.46	n.d	n.d	0.07	n.d	n.d	n.d	0.08	n.d	98.61	1,000.00
	1-128	99.35	0.17	n.d	n.d	0.01	n.d	n.d	0.05	n.d	99.59	998.25
	1-129	99.17	n.d	n.d	n.d	n.d	n.d	n.d	0.03	n.d	99.21	1,000.00
	1-130	99.29	n.d	n.d	n.d	0.01	0.02	n.d	0.04	n.d	99.38	1,000.00
	1-131	100.16	n.d	n.d	0.09	n.d	n.d	n.d	0.05	n.d	100.31	1,000.00
	1-132	98.74	0.47	0.05	n.d	0.01	n.d	n.d	0.14	n.d	99.43	995.19
	1-133	99.45	0.59	n.d	n.d	0.02	0.03	n.d	0.05	n.d	99.62	994.10
	Mean	99.03	0.09	0.00	0.02	0.00	0.01	0.01	0.05	0.00	99.23	999.05
	Max	100.55	1.32	0.09	0.21	0.11	0.07	0.16	0.15	0.30	100.74	1,000.00
	Min	92.55	n.d	n.d	n.d	n.d	n.d	n.d	0.02	n.d	93.61	986.64
	Std. Dev.	0.97	0.19	0.01	0.05	0.01	0.01	0.03	0.02	0.03	0.92	2.00

Notes: Basic statistic parameters—mean, maximum (Max), minimum (Min), and standard deviation (Std. dev.)—are shown;
n.d. = not detected

Appendix Table 2. EPMA Analysis (wt %) of Gold Ore Types in the Las Cruces Supergene Profile

Gold type	Samples	Au	Ag	Cu	Sb	Fe	Se	Pb	S	Hg	Total	Fineness
Gold from breccia-related Au-Ag-rich secondary ore of the cementation zone												
	2-1	74.89	18.39	0.03	0.10	0.04	0.16	0.04	0.15	3.206	97.04	802.81
	2-2	70.52	22.47	n.d	n.d	0.03	0.04	n.d	0.07	6.21	99.36	758.32
	2-3	65.30	25.15	n.d	n.d	0.00	0.04	n.d	0.08	8.35	98.96	721.89
	2-4	88.91	4.86	0.06	0.03	0.03	0.02	n.d	0.13	6.48	100.55	948.15
	2-5	82.02	15.27	n.d	0.01	0.01	0.00	n.d	0.14	1.87	99.34	843.02
	2-6	82.34	14.96	0.04	0.07	0.01	0.03	n.d	0.08	1.599	99.15	846.24
	2-7	78.44	18.54	0.06	n.d	0.10	0.31	n.d	0.63	2.36	99.97	808.82
	2-8	78.71	17.34	0.00	n.d	0.02	0.02	0.15	0.15	2.58	99.00	819.40
	2-9	68.50	23.14	0.03	n.d	n.d	0.01	n.d	0.11	7.49	99.30	747.44
	Mean	76.62	17.79	0.02	0.02	0.03	0.07	0.02	0.17	4.46	99.17	810.68
	Max	88.91	25.15	0.06	0.10	0.10	0.31	0.15	0.63	8.35	100.55	948.15
	Min	65.30	4.86	n.d	n.d	n.d	0.00	n.d	0.07	1.59	97.04	721.89
	Std. dev.	7.54	5.99	0.02	0.03	0.03	0.10	0.05	0.17	2.64	0.95	67.05

Basic statistic parameters—mean, maximum (Max), minimum (Min), and standard deviation (Std. dev.)—are shown)